LBL-1276
c.1

RECEIVED
LAWRENCE
RADIATION LABORATORY

FEB 9 1973

LIBRARY AND
DOCUMENTS SECTION

MÖSSBAUER SPECTROSCOPY OF THE 6.2 keV γ RAY TRANSITION OF ^{181}Ta

Dan Ben Jacov Salomon
(Ph. D. Thesis)

September 1972

Prepared for the U.S. Atomic Energy
Commission under Contract W-7405-ENG-48

For Reference

Not to be taken from this room

LBL-1276
c.1

DISCLAIMER

This document was prepared as an account of work sponsored by the United States Government. While this document is believed to contain correct information, neither the United States Government nor any agency thereof, nor the Regents of the University of California, nor any of their employees, makes any warranty, express or implied, or assumes any legal responsibility for the accuracy, completeness, or usefulness of any information, apparatus, product, or process disclosed, or represents that its use would not infringe privately owned rights. Reference herein to any specific commercial product, process, or service by its trade name, trademark, manufacturer, or otherwise, does not necessarily constitute or imply its endorsement, recommendation, or favoring by the United States Government or any agency thereof, or the Regents of the University of California. The views and opinions of authors expressed herein do not necessarily state or reflect those of the United States Government or any agency thereof or the Regents of the University of California.

MÖSSBAUER SPECTROSCOPY OF THE 6.2 keV γ RAY TRANSITION OF ^{181}Ta

Contents

List of Figures v

List of Tables vii

Abstract ix

I. Introduction 1

II. General Comments 2

A. Mössbauer Effect 2

B. Hyperfine Interactions 3

C. The Case of ^{181}Ta 5

III. Measurement of the Nuclear Magnetic Moment of the 6.2 keV Transition 11

A. Velocity Measurement 11

B. Magnetic Drive 14

C. Mössbauer-NMR 14

The Dispersion Term 19

IV. Nuclear Quadrupole Moment Measurement of ^{181}Ta 20

Nuclear Deformation 23

V. Electric Quadrupole Interactions of ^{181}Ta in Hexagonal Transition Metals 28

VI. Isomer Shifts 37

Systematics of the Isomer Shifts and an Estimate for $\Delta\langle r^2 \rangle$ 43

VII. Temperature Dependence of the Isomer Shifts in Transition Metals 46

VIII. Ta Compounds 53

The Tantalates 54

IX. Hyperfine Interactions of ^{181}Ta in Ni 58

X. Sources and Absorbers Preparations 60

A. Activity 60

B. Sources 61

C. Absorbers 66

Conclusion 69

Appendices 71

I. Mössbauer -- NMR 71

II. Magnetostriction, via rf, Effect on $^{57}Fe(Fe)$ Mössbauer Spectra 81

III. Systematics of Isomer Shifts of ^{57}Fe, ^{197}Au, and ^{99}Ru Impurities in Transition Metals 83

References 87

Acknowledgments 93

LIST OF FIGURES

Fig. 1. Decay scheme for ^{181}Ta 6

Fig. 2. γ-ray energy spectrum for $^{181}W(\underline{W})$ source 8

Fig. 3. Block diagram of electronic components 10

Fig. 4. Single-line and magnetically-split velocity spectra for $^{181}W(\underline{W})$ 13

Fig. 5. Magnetic drive spectrum for $^{181}W(\underline{W})$ 15

Fig. 6. Frequency spectrum for Mössbauer NMR in $^{181}W(\underline{W})$ 17

Fig. 7. Line position graph for the 9/2 — 7/2 E1 transition as a function of Q(9/2)/Q(7/2) 21

Fig. 8. Velocity spectra of ^{181}Ta in Re single crystal 22

Fig. 9. Velocity spectra in hexagonal hosts of Re, Os, and Ru . . 29

Fig. 10. Velocity spectra in hexagonal hosts of Os and single crystal Ru 30

Fig. 11. Velocity spectrum in hexagonal host of Hf metal 31

Fig. 12. Velocity spectra of TaC, $KTaO_3$, and Ta metal absorber ($^{181}W(\underline{W})$ source), and of Mo host 38

Fig. 13. Single-line velocity spectra of Ni, Mo, Nb, Ir, W, and Pt hosts 39

Fig. 14. Single-line velocity spectra of V, Rh, Pd, and Ta hosts 40

Fig. 15. Graphical representation of the isomer shifts of ^{181}Ta 42

Fig. 16. Systematics of the isomer shifts for ^{181}Ta 44

Fig. 17. Experimental arrangement for temperature studies 47

Fig. 18. Experimental results for the shifts of the isomer shifts 48

Fig. 19. Velocity spectra for $LiTaO_3$ absorber 55

Fig. 20. Velocity spectra for the tantalates absorbers $LiTaO_3$, $NaTaO_3$, and $KTaO_3$ 56

Fig. 21. Velocity spectra for $^{181}W(Ni)$ source above the Curie pt. and at 298 K 59

Fig. 22. rf heating arrangement for sources preparations 62

Fig. I-1. Theoretical velocity spectra with rf for ^{57}Fe 75

Fig. I-2. Theoretical frequency spectra for ^{57}Fe 77

Fig. I-3. Experimental result for ^{57}Fe 78

Fig. I-4. Theoretical frequency spectra for ^{181}Ta 79

Fig. I-5. Experimental result for ^{181}Ta 80

Fig. II-1. rf (magnetostriction) effects on ^{57}Fe velocity spectrum 82

Fig. III-1. Systematics of isomer shifts for ^{57}Fe 84

LIST OF TABLES

Table 1. Relative intensities of the individual components ($9/2 \rightarrow 7/2$ E1) 12

Table 2. Experimental results for $g(9/2)/g(7/2)$ and 2ξ 18

Table 3. Experimental results for $Q(9/2)/Q(7/2)$ 24

Table 4. Experimental results for EFG in hexagonal transition metal hosts 32

Table 5. Comparison of EFG with theoretical treatment 34

Table 6. Comparison with other measurements of EFG in hexagonal transition metals 36

Table 7. Isomer shifts results 41

Table 8. Temperature shifts results of isomer shift in transition metals 50

Table 9. Summary of experimental results for the tantalates 57

Table 10. Comparison of Ta/Nb sites in $LiTaO_3$ 57

Table 11. Fluxes where sources were irradiated 60

Table 12. Source preparation data 64

Table 13. Comparison of ^{181}Ta with other Mössbauer transitions . . 70

MÖSSBAUER SPECTROSCOPY OF THE 6.2 keV γ RAY TRANSITION OF ^{181}Ta

Dan Ben Jacov Salomon

Department of Physics and
Lawrence Berkeley Laboratory
University of California
Berkeley, California 94720

September 1972

ABSTRACT

Recoilless nuclear resonance absorption of the 6.2 keV γ rays of ^{181}Ta, was used for the hyperfine interactions of dilute ^{181}Ta impurities in the 5d, 4d, and 3d transition metals (Hf, Ta, W, Re, Os, Ir, Pt, Nb, Mo, Ru, Rh, Pd, V, and Ni) and the Ta compounds $LiTaO_3$, $NaTaO_3$, $KTaO_3$, and TaC. Ratios of the nuclear parameters of the 6.2 keV excited state (I = 9/2) to the ground state (I = 7/2) were derived from completely resolved magnetic and electric-quadrupole split spectra:

$$g(9/2)/g(7/2) = 1.77 \pm 0.02$$

$$Q(9/2)/Q(7/2) = 1.133 \pm 0.010$$

and estimates for the mean-square nuclear charge radius were obtained:

$$\Delta \langle r^2 \rangle \begin{cases} \sim -1.6 \text{ fm}^2 \\ \sim -4.5 \text{ fm}^2 \end{cases} .$$

The measured isomer shifts covered a range of 110 mm/s, corresponding to 17,000 times the natural line-width or more than 1,600 times the best experimental line-width of the 6.2 keV transition. In addition, both the sign and the magnitude of the electric field gradient

were measured in the hexagonal transition metals Hf, Re, Os, and Ru, and in the tantalum compounds $LiTaO_3$ and $NaTaO_3$. Temperature studies of the isomer shifts in the transition metals, Ta, W, Ir, Pt, Mo, Pd, and Ni, were carried out, showing shifts of the isomer-shifts much larger than the second order Doppler shift.

Mössbauer-NMR is reviewed in connection with the ^{181}Ta resonance.

I. INTRODUCTION

The 6.2 keV γ ray transition of ^{181}Ta has been a target for Mössbauer studies since it was first observed by Muir and Boehm [1]. A few (published [2,3] and unpublished) attempts were made, but it was Sauer et al. [4,5] who finally observed a true tantalum resonance. Present work shows that ^{181}Ta is indeed the most "powerful" Mössbauer nucleus for hyperfine, solid state, and Ta - chemistry studies.

^{181}Ta has the lowest transition energy of any anticipated or observed Mössbauer decay, and also has a relatively long half-life of 6.8 μs for the excited state. These properties alone predict an almost 100% Mössbauer effect with an extremely high resolution of natural line-width, $\Gamma_o = 6.7 \times 10^{-11}$ ev.

Although the best experimental cases of ^{181}Ta resonance have widths of the order of 20 times the natural width and measured effects of only a few percent, ^{181}Ta is still the best Mössbauer transition for high resolution work. This is due to the fact that the nuclear parameters involved for both excited and ground state are very large. This high sensitivity, on the other hand, creates difficulties in observing the resonance, as it is extremely vulnerable to impurities and lattice defects.

II. GENERAL COMMENTS

A. Mössbauer Effect

While there are several reviews on the Mössbauer effect, [e.g. 6, 7,8,9], only few relevant aspects will be pointed out here.

Recoilless nuclear resonance absorption, as one may call the Mössbauer effect, comes about when the γ ray, corresponding to a nuclear decay to its ground state, is emitted without energy loss due to nuclear recoil or Doppler broadening due to thermal motion. This condition is met when the emitting nucleus is embedded in a crystalline material, thus impairing the recoil momentum to the crystallite as a whole. Similarly, this "coherent" γ ray which has an energy spread (width) $\Gamma_o = \hbar/\tau$, where τ is the life time of the excited state, can be absorbed by an absorber containing the same nuclei in their ground state. One, therefore, has a nuclear resonance fluorescence.

In the case of ^{57}Fe, the 14.4 keV transition has a width $\Gamma = 4.7 \times 10^{-9}$ ev and for ^{181}Ta the natural width is $\Gamma_o = 6.7 \times 10^{-11}$ ev. While Mössbauer absorption does not measure the absolute values of the transition energy, it can measure shifts within several orders of magnitude of the line width. To measure these shifts, one notes that Doppler velocities of the order of mm/s (v) produce shifts $\Delta E = E(v/c)$, where E is the γ ray energy and c is the speed of light. For ^{181}Ta, 1 mm/s corresponds to $\sim 2 \times 10^{-8}$ ev.

In general, the fraction of recoil-free events is given in the Debye model by the f-factor:

$$f = \exp\left\{ - \frac{6E_R}{k\theta_D} \left[\frac{1}{4} + \frac{T^2}{\theta_D} \int_0^{\theta_D/T} \frac{x\,dx}{e^x - 1} \right] \right\} \tag{1}$$

where T is the temperature (K), θ_D is the Debye temperature of the host crystal, and $E_R = E_\gamma^2/2Mc^2$, M being the mass of the nucleus. For ^{181}Ta, because of the high mass and the low γ ray energy of 6.2 keV, f is nearly unity up to 1,000 K. Clearly, this makes ^{181}Ta an excellent case for high-temperature studies.

As a final remark, the absorption line is a Lorentzian curve, given by

$$\sigma(E) \sim \sigma_o \frac{(\Gamma/2)^2}{(E - E_o)^2 + (\Gamma/2)^2} \tag{2}$$

where Γ is the total absorption line width, and σ_o is the effective resonance cross section

$$\sigma_o = 2\pi\lambda^2 \left(\frac{2I' + 1}{2I + 1}\right)\left(\frac{1}{1 + \alpha}\right)$$

where I' and I are the spins of the excited and ground states, respectively, λ is the wave length of the radiation, and α is the internal conversion coefficient. For ^{181}Ta, α is 46±8 [10], and, as will be discussed in section III, the Lorentzian absorption line is modified by a dispersion term.

B. Hyperfine Interactions

One can describe the interaction of the nucleus with its surroundings in a solid by the hamiltonian $H = H_{IS} + H_M + H_Q$.

The first term, H_{IS}, is the electric monopole component of the coulombic interaction:

$$W_e = -e^2 \iint \frac{\rho_n(r_n)\cdot\rho_e(r_e)}{|r_e - r_n|} d\tau_e d\tau_n \quad , \tag{3}$$

where the subscripts n and e refer to the nucleus and the electron. As is shown below, this interaction leads to the isomer shift, which in essence measures differences of charge densities at the nucleus - the most unique feature of the Mössbauer effect. H_M is the magnetic interaction or Zeeman splitting, $-\underline{\mu}\cdot \underline{H}_{eff}$, (see section III). And H_Q is the electric quadrupole interaction with the electric field gradient, (see section IV).

The Isomer Shift

If one considers a simple nuclear decay of transition energy E_o from an excited state B to a ground state A, one can then evaluate equation (3) for state B and for state A. This would shift the states A and B by a small amount of energies W_A and W_B, respectively, giving a net shift δ_s to E_o:

$$\delta_s = \frac{2\pi}{3} Ze^2 |\psi_o|_s^2 (\langle r_E^2 \rangle - \langle r_G^2 \rangle)$$

Here $|\psi_o|_s^2$ is the electron density at the nucleus, and $\langle r_E^2 \rangle$ and $\langle r_G^2 \rangle$ are the excited and ground state mean square nuclear charge radii. If one considers δ_s to be the shift for the emitting nucleus (source), then one can derive a similar expression for the absorbing nucleus (absorber), δ_a. The net energy difference is then

$$\delta_a - \delta_s = (\frac{2\pi}{3})\ Ze^2\ (|\psi_o|^2_a - |\psi_o|^2_s)(\langle r_E{}^2 \rangle - \langle r_G{}^2 \rangle) \qquad (4)$$

This expression is called the isomer shift (IS) of the absorber with respect to the source.

Equation (4) is more compactly written as†

$$IS = (\frac{2\pi}{3})\ Ze^2\ \Delta|\psi_o|^2\ \Delta\langle r^2 \rangle \qquad (5)$$

or for ^{181}Ta,

$$IS = 1.056\ 10^3\ \Delta|\psi_o|^2\ \Delta\langle r^2 \rangle \quad , \qquad (6)$$

where the IS is in mm/s, $\Delta|\psi_o|^2$ is in 10^{26} cm^{-3}, and $\Delta\langle r^2 \rangle$ is in fm^2 (= 10^{-26} cm^2).

C. <u>The Case of ^{181}Ta</u>

In this part the experimental aspects in regard to the ^{181}Ta resonance are presented, especially the problem of observing the 6.2 keV γ rays.

<u>The Decay Scheme</u>

The decay scheme for ^{181}Ta is shown in Fig. 1. The two main levels used for hyperfine interactions are the 6.2 keV (present work) and the 482 keV [12]. The 6.2 keV level is studied with the Mössbauer technique, while the 482 keV level is pursued by time-differentiated-perturbed-

---

†This expression is subject to relativistic corrections [11].

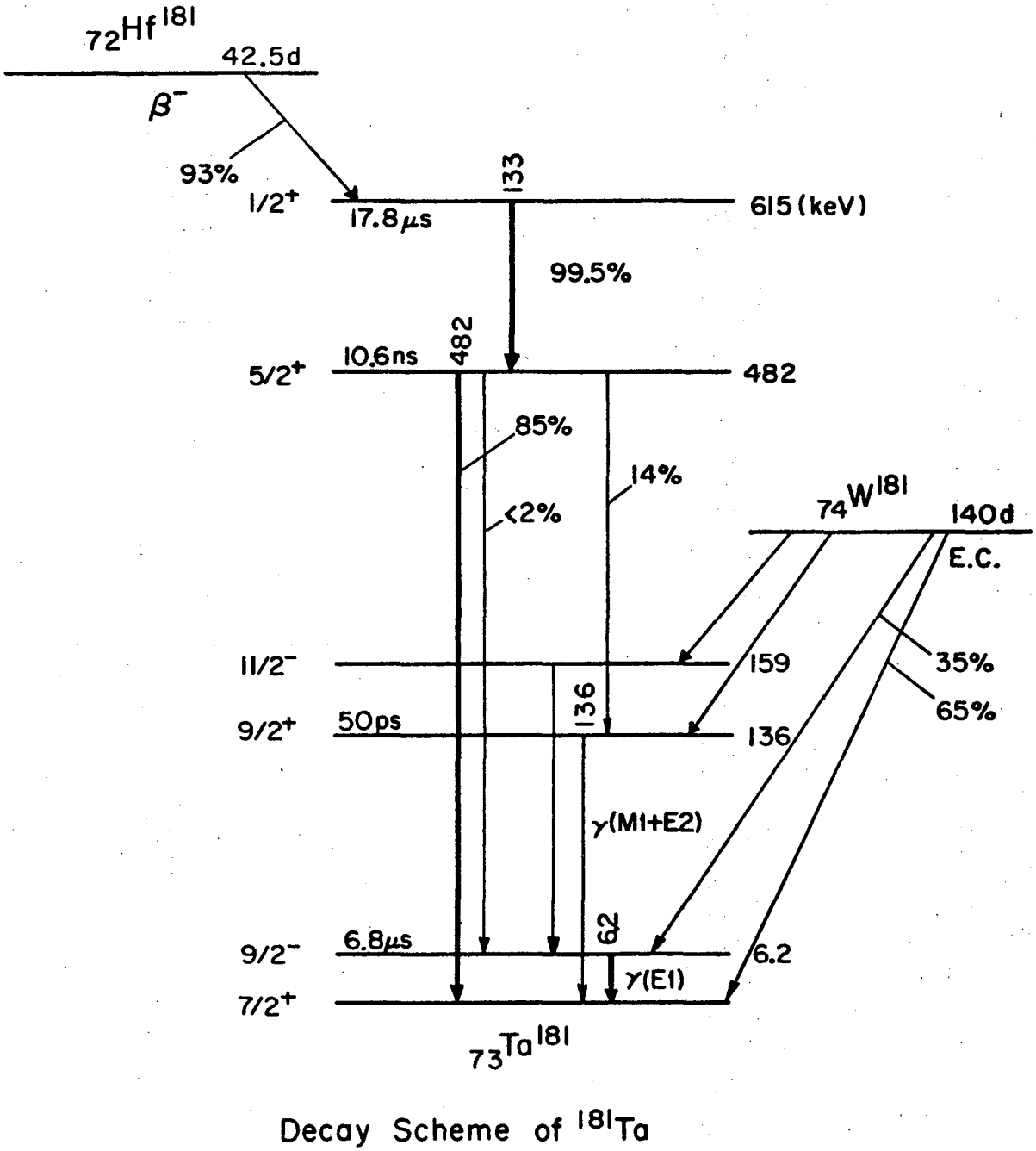

Decay Scheme of ^{181}Ta

XBL728-3806

Fig. 1. The decay scheme for the ^{181}Ta nucleus (Lederer et al. [14]). The 6.2 keV Mössbauer transition and the 133-482 keV transitions for TDPAC are indicated by the heavy lines.

angular-correlation (TDPAC). These two processes can compete for electric field gradient studies (see section V). As a passing note, one should mention that the 136 keV level is also a Mössbauer transition [13]. However, due to its short life time of 50 ps and small effect (due to the high energy), its usefulness is very limited.

The 6.2 keV line can be populated, as can be seen from Fig. 1, via ^{181}Hf β decay and ^{181}W electron capture. The ^{181}W case is extremely favorable; it has a longer parent life time and it decays directly to the 6.2 keV level (35%) without the production of appreciable high energy γ ray background. The ^{181}Hf "route" produces high energy background, and the population of the 6.2 keV level is so poor that it is hopeless even to observe the 6.2 keV γ ray† in an energy spectrum. All sources in this work were prepared from ^{181}W activity, (see section X).

Detectors

To detect the 6.2 keV γ rays an argon - 10% methane refillable proportional counter was used. Figure 2 shows the γ ray spectrum for the ^{181}W source detected by a proportional counter and a Si(Li) diode detector. Although the resolution of the Si(Li) detector is excellent, it is not suitable for the Mössbauer work. The spectrum shown here (Fig. 2) was taken for a source without a Ta-metal absorber. The absorber diminishes the 6.2 keV peak with respect to the steady background (not shown here), to a ratio of less than 1 to 2. Also the counting rate for the 6.2 keV peak was very low, less than 10 counts/s. Both resolution

†For the 6.2 keV level the internal conversion factor is ~ 46, so that the γ rays of the level are completely hidden by the rest of the decay.

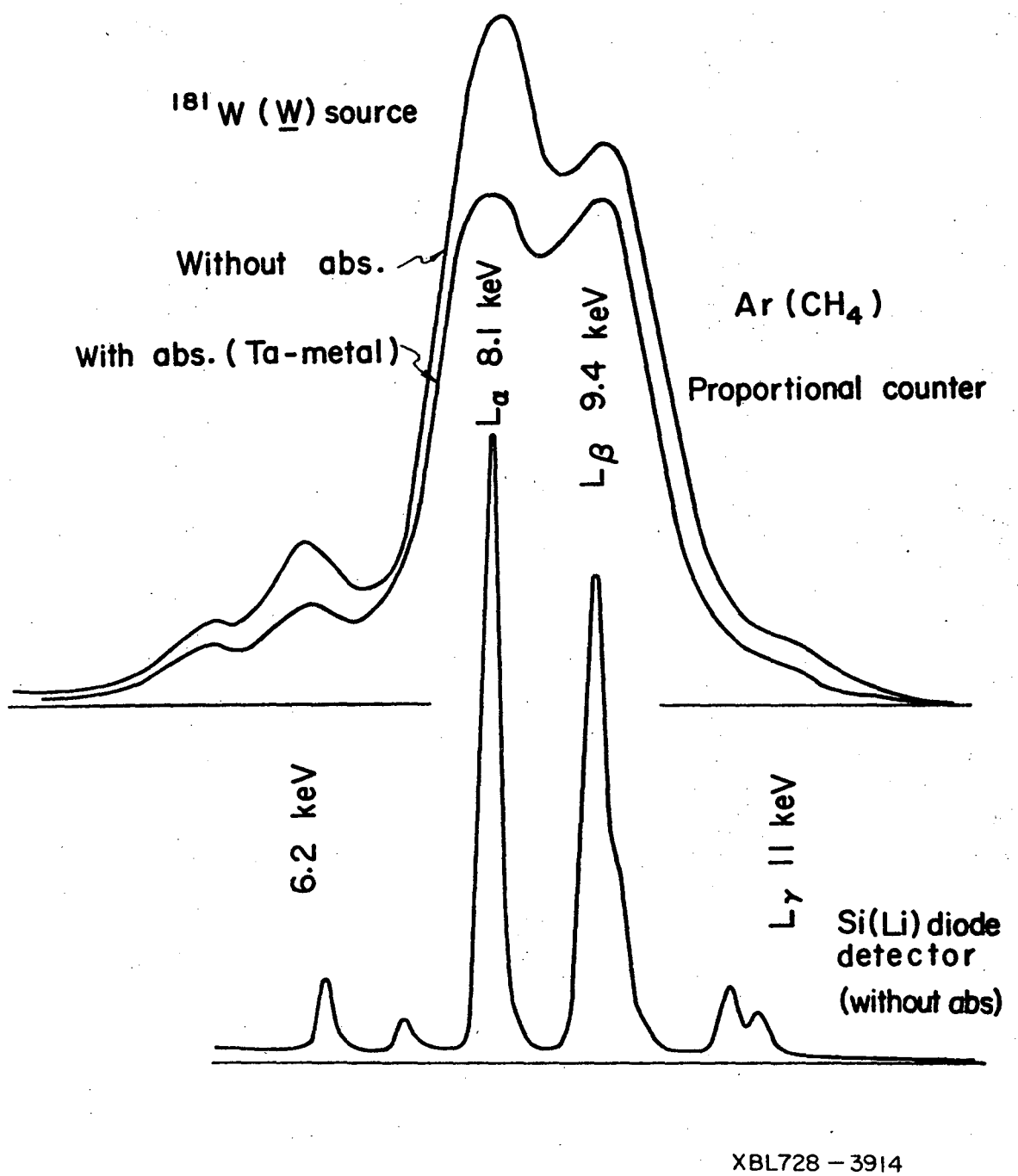

Fig. 2. γ ray energy spectra for ^{181}W(W) source as seen by a proportional counter (above) and a Si(Li) detector (below). The energy scales are not identical.

and background become progressively worse as the count rate increases. This is to be contrasted with the high (now standard) count rate of 2,000 counts/s for the proportional counter.

The proportional counters used were filled to 1.5 atmospheres of pressure with an argon - 10% methane gas mixture. Different gas mixtures with neon and krypton did not improve in efficiency at the high counting rates mentioned above. The 3 keV escape peak of argon for the W - L_β X-ray is the main background for the 6.2 keV peak. In spite of this, the argon-filled proportional counter is the best detector for the 6.2 keV Mössbauer work.

Experimental Arrangement

In all velocity experiments a sinusoidal electro-mechanical drive [15] was used. The entire assembly of drive, source, and absorber was rigidly mounted in an evacuated can to avoid vibrational and acoustical disturbances. A 3 mil beryllium window made the observation of the 6.2 keV γ rays possible without much attenuation. The schematic of the electronics is shown in Fig. 3. The multichannel analyzers used had 400 channels and 2048 channels. The latter was needed for the high resolution cases.

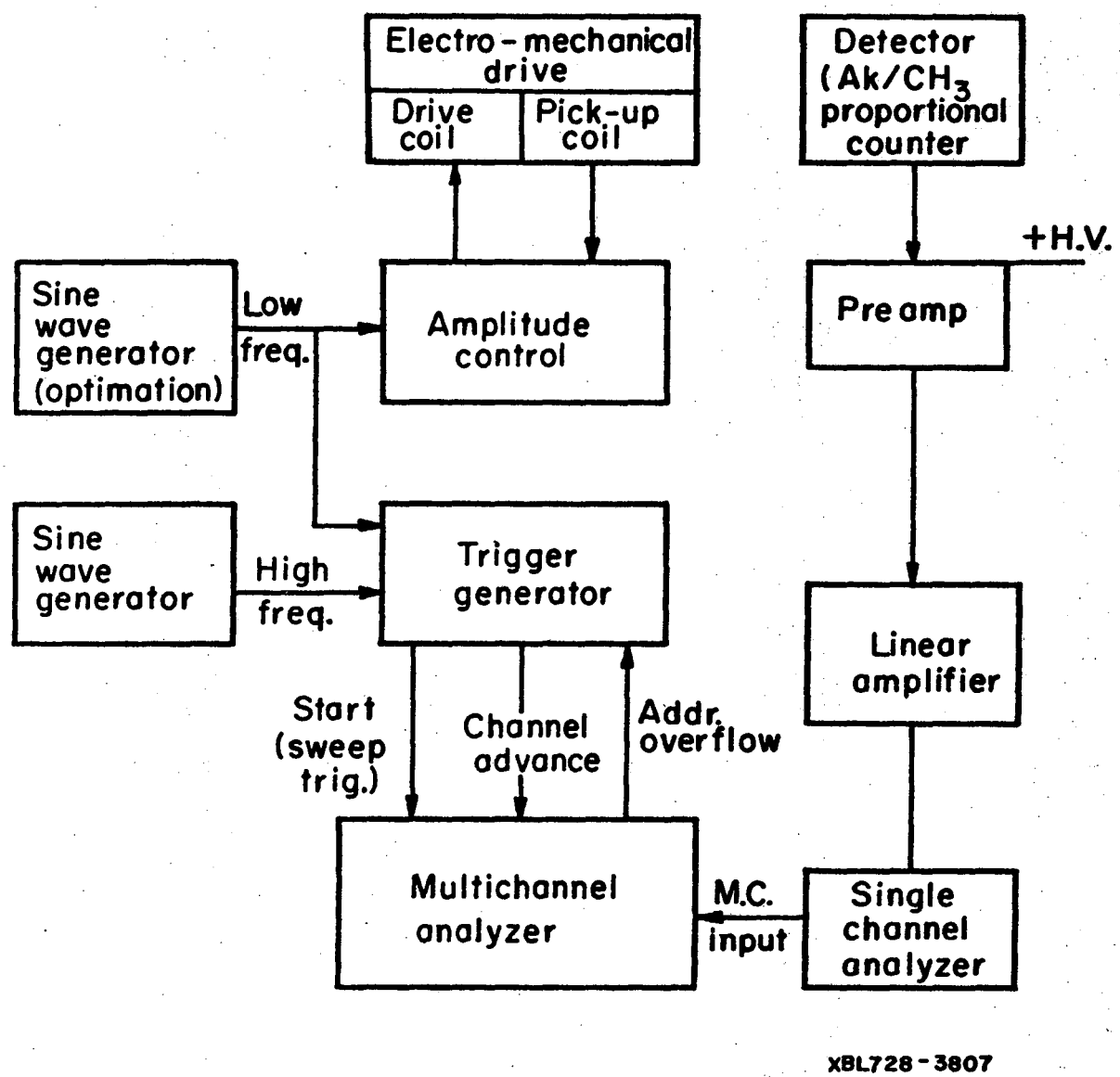

Fig. 3. Block diagram of the electronic components.

III. MEASUREMENT OF THE NUCLEAR MAGNETIC MOMENT OF THE 6.2 keV TRANSITION

The excited state of ^{181}Ta has a spin I of 9/2 and decays via an E1 transition to the ground state which has a spin I of 7/2. In a magnetic field this transition splits into 24 components, of which 16 are $\Delta m = \pm 1$ and 8 are $\Delta m = 0$. The relative intensities are given by the Clebsch-Gordon coefficients and the $F_M^{LL}(\theta)$ function [16]. Table 1 shows the relative intensities of the components for $\theta = 0°$ and $\theta = 90°$, θ being the angle between the direction of the magnetic field and the observation direction. Three experiments were carried out to measure the magnetic splitting.

A. Velocity Measurement

The source ^{181}W(W)† was mounted on a small Sm-Co permanent magnet. The magnet was a cylinder 3/4 inch in diameter and 3/4 inch long, and produced a magnetic field at the center of the flat end of 2.93±0.03 kOe. The Ta metal absorber was kept at zero magnetic field [17]. Figure 4 shows the velocity spectra for a single line (zero field) and split spectra.

The spectra exhibit a distinct asymmetry, which is due to the interference effect between photoelectric absorption and nuclear resonance absorption followed by internal conversion. This gives rise to a dispersion term, ξ, which is discussed at the end of this section. The curves in Fig. 4 were least squares fitted with the theoretical curve [18,19]

---

†This source was the first one to exhibit clearly the tantalum resonance, (see section X).

Table 1. Relative intensities of the individual components of the E1 6.2 keV 9/2 → 7/2 transitions. θ is the angle between the magnetic field (axis of quantization) and the direction of observation.

m_i	m_f	$C\begin{pmatrix} 9/2 & 7/2 & I \\ m_i & -m_f & M \end{pmatrix}$	θ = 0°	θ = 90°
-9/2	-7/2	36	same	same
-7/2	-5/2	28		
-5/2	-7/2	1		
-5/2	-3/2	21		
-3/2	-5/2	3		
-3/2	-1/2	15		
-1/2	-3/2	6		
-1/2	+1/2	10		
+1/2	-1/2	10		
+1/2	+3/2	6		
+3/2	+1/2	15		
+3/2	+5/2	3		
+5/2	+3/2	21		
+5/2	+7/2	1		
+7/2	+5/2	28		
+9/2	+7/2	36		
-7/2	-7/2	8	0	16
-5/2	-5/2	14		28
-3/2	-3/2	18		36
-1/2	-1/2	20		40
+1/2	+1/2	20		40
+3/2	+3/2	18		36
+5/2	+5/2	14		28
+7/2	+7/2	8		16

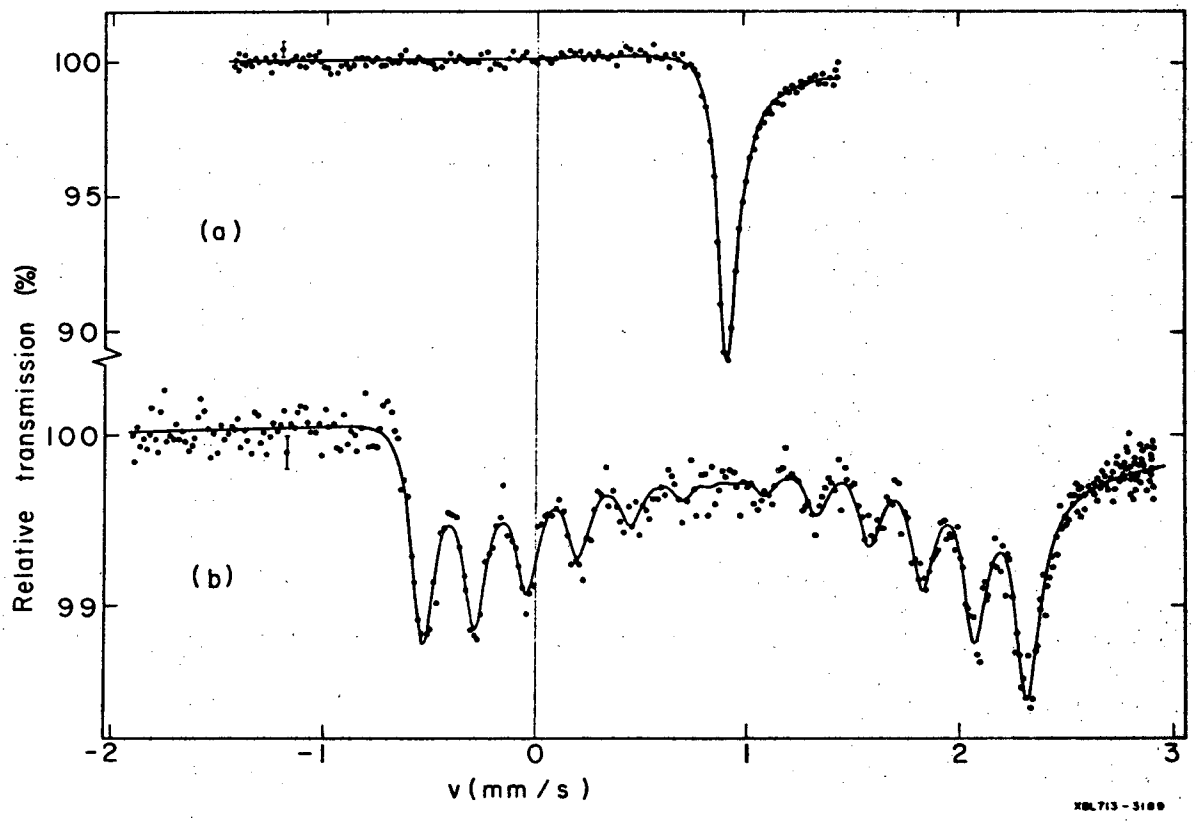

Fig. 4. Velocity spectra of the 6.2 keV γ transition for ^{181}W(W) source and a single-line Ta-metal absorber. (a) unsplit source. (b) source in a longitudenal magnetic field of 2.93±0.02 kOe.

$$N(v) = N(\infty) - A(1 - 2\xi X)/(1 + X^2)$$
$$X = 2(v - v_o)/W \quad . \tag{7}$$

Here, $N(v)$ is the intensity transmitted at relative velocity v, v_o is the position of the line, W is the full line width at half-maximum, and A is the amplitude of the line.

From the fit one obtains a g-factor ratio of $g(9/2)/g(7/2) = 1.78 \pm 0.02$.

B. Magnetic Drive

One notes from Fig. 4 that due to the isomer shift of $^{181}W(\underline{W})$ source with respect to Ta metal, the outer lines of the split spectra will pass through the zero velocity position as the applied magnetic field is increased. In fact, one can write the position at zero velocity as a function of the magnetic field H as follows:

$$I.S. = \mu_N g_o H[-(g_1/g_o)m_1 + m_o] \quad .$$

Thus, an experiment at zero velocity using a variable magnetic field was performed. The source, $^{181}W(\underline{W})$, was placed in a magnetic field which was varied from 1.5 to 4.5 kOe, while the absorber was kept at zero magnetic field [17]. The resultant spectrum, shown in Fig. 5, yielded a value of $g(9/2)/g(7/2) = 1.76 \pm 0.04$ for the g-factor ratio.

C. Mössbauer-NMR

While the idea of Mössbauer-NMR is discussed in great detail in Appendix I, only the experimental results will be noted here [20]. One

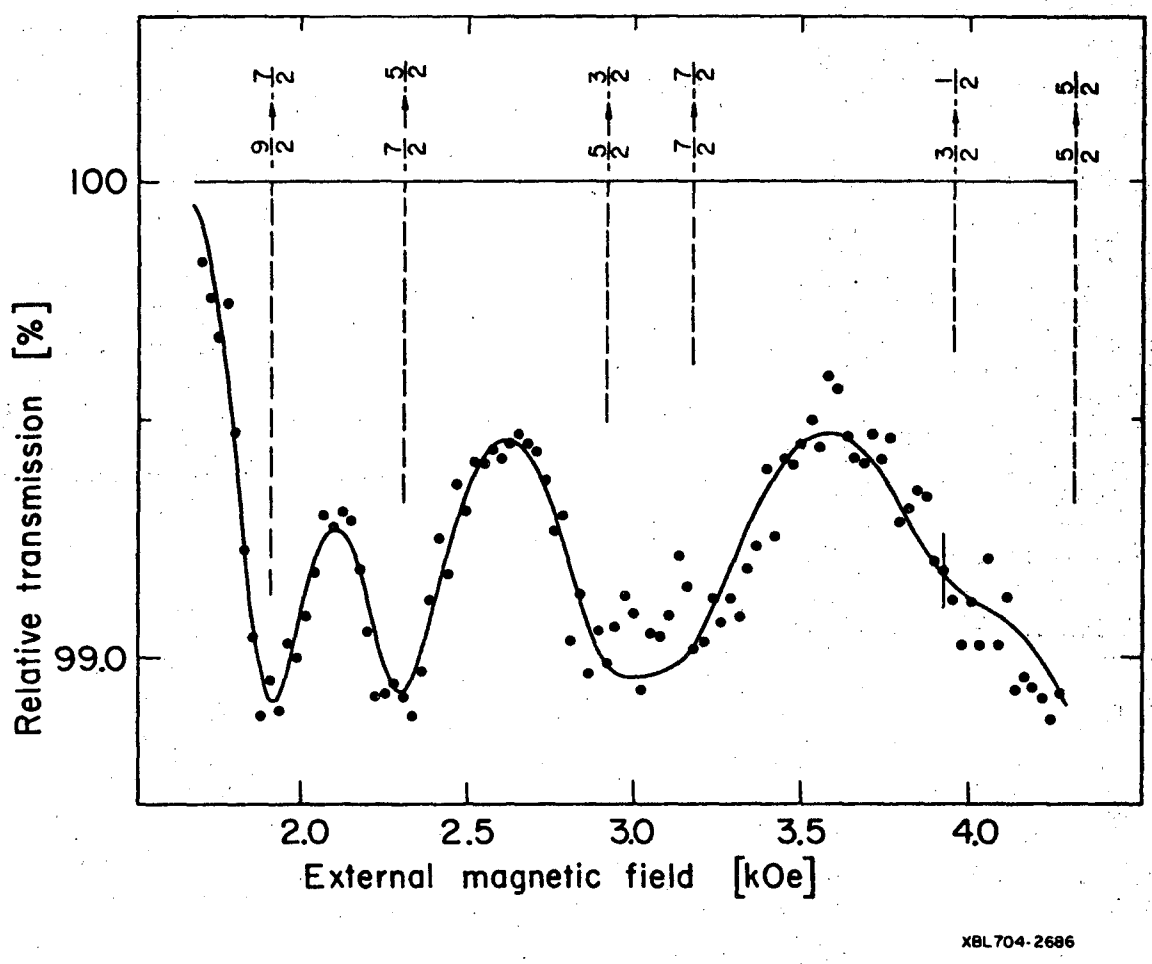

Fig. 5. Absorption spectrum of the 6.2 keV γ transition, measured with a "magnetic drive" for a $^{181}W(\underline{W})$ source in the magnetic field and a single-line Ta-metal absorber outside the field. The position and intensities of the components are indicated by broken lines.

notes from Fig. 5 that in an external field of 1800 Oe, only the $-9/2 \rightarrow -7/2$ component of the split source is at the zero velocity position with respect to the Ta absorber. If one now applies a radiofrequency field to the source one expects induced transition between the levels at the resonant frequencies. An experiment was carried out at zero velocity and fixed H_o as shown in Fig. 6. Clearly the accuracy of the measurement here, due to the small effect, was not high; but the value of $g(9/2)/g(7/2) = 1.83 \pm 0.08$ deduced is in good agreement with the two previous measurements.

The results of all three methods are summarized in Table 2. While the velocity spectrum is of highest accuracy, one should not ignore the results of the other two spectra, which were done more as explorations in methodology.

The Nuclear Magnetic Moment

From Table 2 a weighted average for the g-factor ratio results in

$$g(9/2)/g(7/2) = 1.77 \pm 0.02 \quad .$$

Using $\mu(7/2) = (2.35 \pm 0.01)\mu_N$ [21], one gets for the 6.2 keV state

$$\mu(9/2) = (5.35 \pm 0.09)\mu_N \quad .$$

The 6.2 keV state has been classified [22] as the [514] Nilsson state which is the same as the 206 keV state in ^{187}Re, for which the magnetic moment has been measured as $(5.02 \pm 0.06)\mu_N$ [23] and as $(4.71 \pm 0.14)\mu_N$ [24]. These values are somewhat smaller than the one for ^{181}Ta. Also, the theoretical prediction of the Nilsson model, with a deformation parameter $\delta = 0.26$, indicates a value of $\mu = 5.08\ \mu_N$ [25].

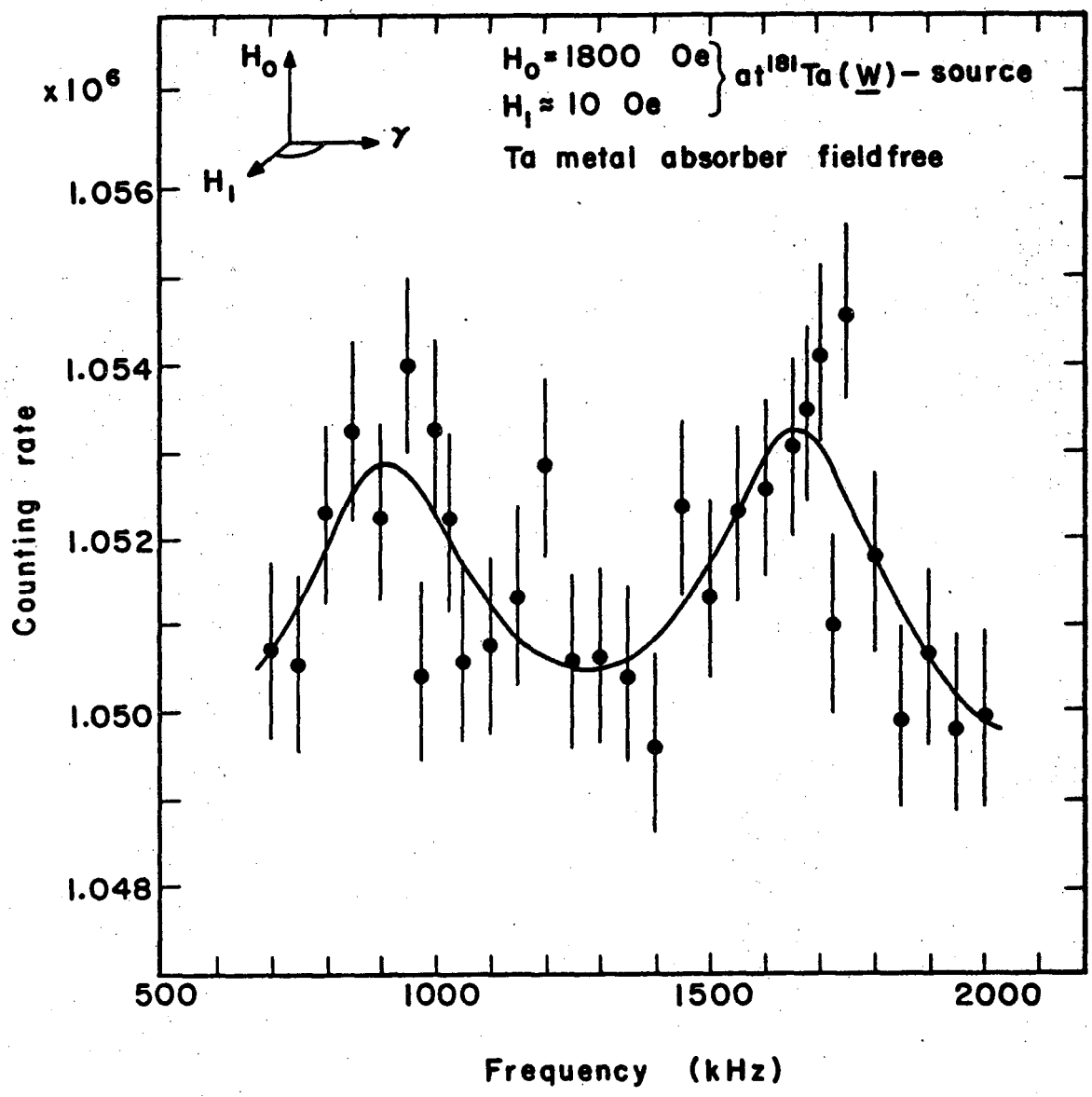

XBL713-3188

Fig. 6. Frequency spectrum of the set-up shown above. (rf off count rate is 1.051×10^6.)

Table 2. Summary of experimental results obtained for a single-line Ta absorber and an unsplit and split $^{181}W(\underline{W})$ source.

	Velocity spectra			
	unsplit	magnetically split	Magnetic drive spectrum	Mössbauer NMR
W/2 (mm/s)	0.056±0.001	0.066±.002	0.069±0.003	0.04±0.02
2ξ	-0.31±0.01	-0.31±0.01	-0.35±0.07	---
IS (mm/s)	0.857±0.005	0.854±0.005	---	---
g(9/2)/g(7/2)	---	1.78±0.02	1.76±0.04	1.83±0.08

The Dispersion Term

The dispersion term (ξ) represents the interference of the photoelectric absorption and the nuclear resonance absorption followed by internal conversion. This is a phenomenon which takes place at the absorber [18,19]. The total cross section is then given by

$$\sigma = \frac{\sigma_o}{1 + X^2} (1 - 2\xi X) + \sigma_e \tag{8}$$

X is the same as in equation (7), σ_e is the atomic photoelectric cross-section, $\sigma_o/(1 + X^2)$ is the Mössbauer resonance, and $2\cdot\xi\cdot X\sigma_o/(1 + X^2)$ is the interference term.

The expression for ξ is given by Trammel et al. [18] as

$$\xi = \varepsilon \left(\frac{\alpha\, \sigma_1^{\,1}}{6\pi\, \lambda\!\!\!^{-2}} \right)^{1/2} ,$$

where $\sigma_1^{\,1}$ is the partial cross-section for E1 photoelectric absorption, α is the internal conversion coefficient, and $\lambda\!\!\!^{-}$ is the wavelength of the incident γ rays, divided by 2π. The coefficient ε is introduced to account for the fact that α and $\sigma_1^{\,1}$ are proportional to the sum of the squares of transition amplitudes to various final states, while ξ is proportional to the sum of the products of these amplitudes [18].

For ^{181}Ta, one has $\alpha = 46\pm8$ [10], $\sigma_e^{\,1} \cong \sigma_e = 9.8\ 10^4$b [26]. Thus, one obtains a theoretical value $2\xi = 0.31\ \varepsilon$. Comparing with the results in Table 2, it follows that ε is very close to 1.

IV. NUCLEAR QUADRUPOLE MOMENT MEASUREMENT OF ^{181}Ta

The nuclear quadrupole moment, Q, interacts with an electric field gradient (EFG), $q(=\partial^2 V/\partial^2 z)$, via the Hamiltonian [27],

$$H_Q = \frac{eqQ}{4I(2I-1)} \{3I_z^2 - I(I+1) + \eta(I_x^2 - I_y^2)\} \qquad (9)$$

where the asymmetry parameter is given by

$$\eta = \left(\frac{\partial^2 V}{\partial^2 x} - \frac{\partial^2 V}{\partial^2 y}\right) \Big/ \left(\frac{\partial^2 V}{\partial^2 z}\right) .$$

In order to observe this interaction, the ^{181}Ta nucleus was used as an impurity in a hexagonal single crystal host of Re metal, (see section X). In this case, one assumes η to be zero due to the axial symmetry of the EFG of the host. The quadrupole splitting gives then 4 levels for the ground state and 5 levels for the 6.2 keV state; giving rise to 11 components for the γ transition: seven with $\Delta m = \pm 1$, three with $\Delta m = 0$, and one mixed.

Figure 7 shows the line position as a function of the quadrupole ratio, Q(9/2)/Q(7/2), for two different geometries with respect to the axis of symmetry of the EFG. In one case, (Fig. 7a), the observation direction $\underline{k}$ is perpendicular to the axis of the EFG; in the other case, (Fig. 7b), $\underline{k}$ is parallel to the EFG axis. The measured velocity spectra are shown in Fig. 8. Although the line widths are about 100 times the natural line width, the spectrum is well resolved and in agreement with the curves of Fig. 7, as is indicated by the broken lines. The curves

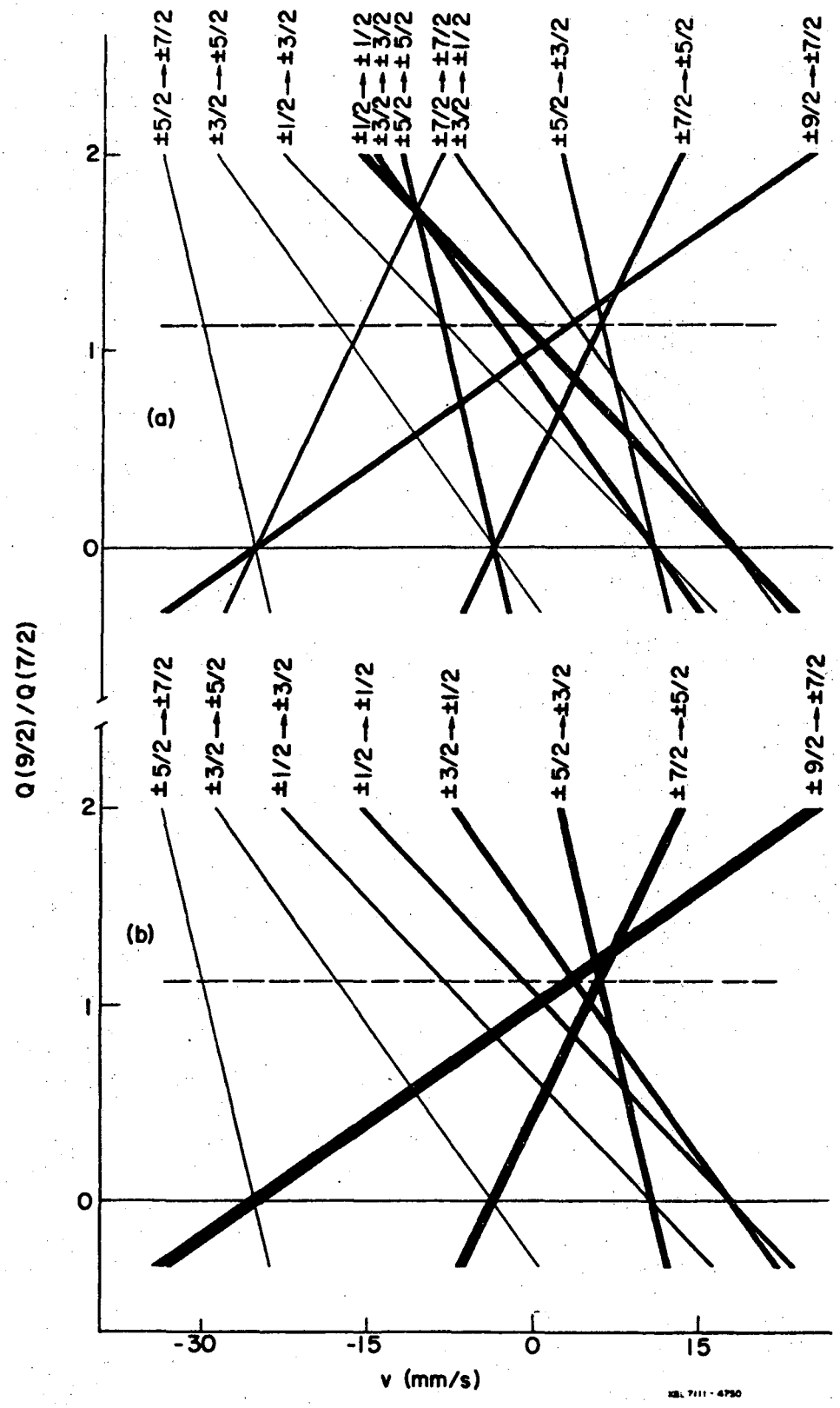

Fig. 7. Graphical presentation for expected line position for the 9/2 → 7/2 (E1) transition in ^{181}Ta as a function of the quadrupole moments ratio, Q(9/2)/Q(7/2), in an axially symmetrical EFG. (a) For the direction of observation perpendicular to the axis of the EFG, (b) parallel to it. The widths of the lines are proportional to the relative intensities of the components.

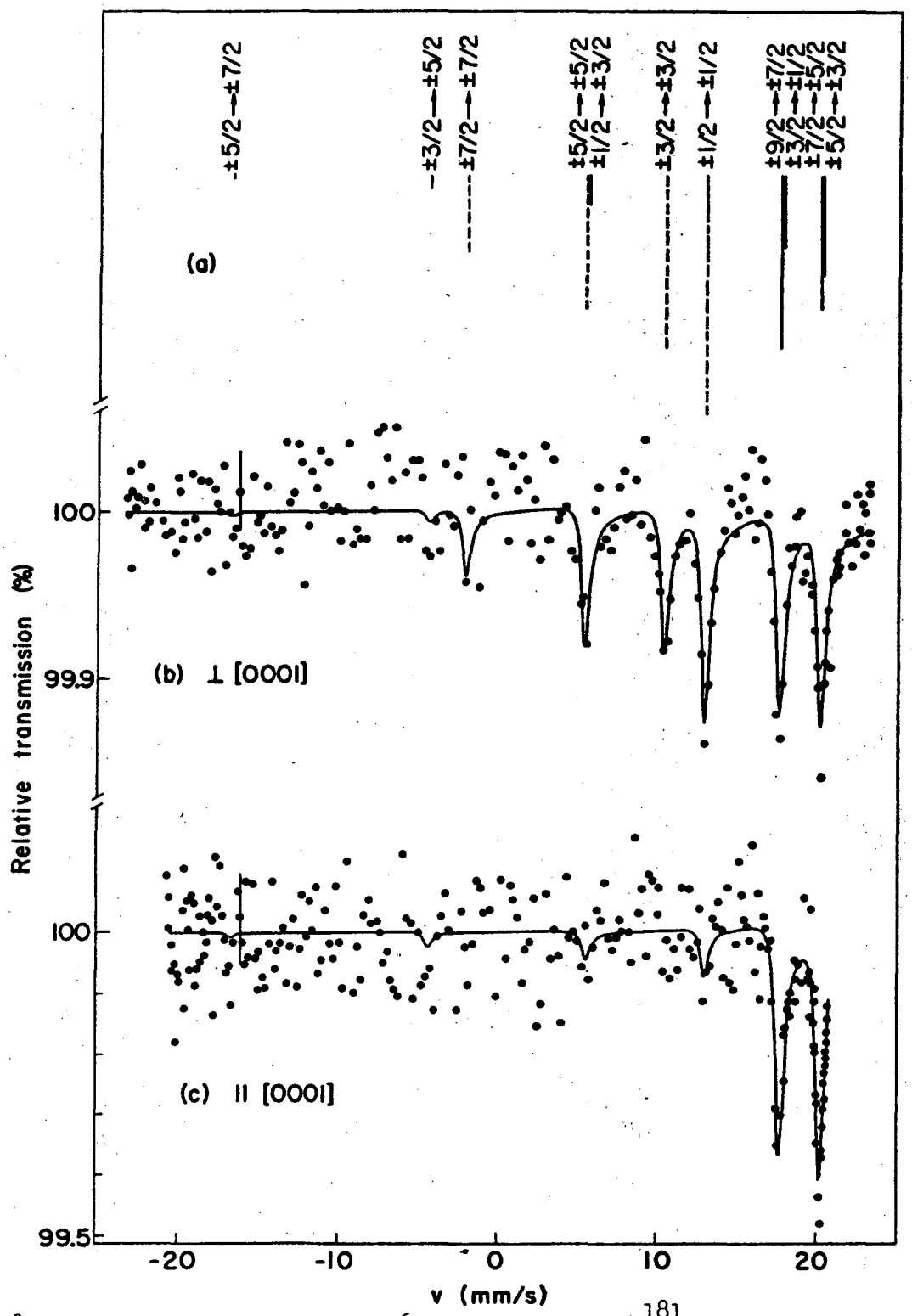

Fig. 8. Velocity spectra of the 6.2 keV γ rays of ^{181}Ta in a single crystal Re metal, versus a Ta-metal single line absorber. Observation direction is perpendicular in (b), and in (c) parallel to the [0001] axis. The results of a simultaneous least-square-fit of both spectra are shown by solid lines. In (a) the position and relative intensities are shown for the various components; solid lines for $\Delta m = \pm 1$, and broken lines $\Delta m = 0$ (perpendicular to [0001] axis) transitions.

were fitted simultaneously by least-squares-fit with a superposition of dispersion modified Lorentzian lines;

$$N(v) = N(\infty) \left\{ 1 - \sum_{\substack{i=1,\\ 11}} \frac{A(i)(W/2)^2}{(v - v_o(i))^2 + (W/2)^2} \left(1 + 2\xi \frac{v - v(i)}{W/2}\right) \right\} \tag{10}$$

The notation here is the same as in equation (7).

The experimental results of the least-square-fit of the spectra in Fig. 8 are shown in Table 3. It should be noted that, in addition to the isomer shift, the quadrupole moment ratio, and the EFG, the sign of the EFG was also obtained [28]. The discussion of EFG is left for the next section.

The electric quadrupole moment of the $7/2^+$ ground state was measured by Lindgren [29] to be $Q(7/2) = (+\ 3.9 \pm 0.4)$b. Using the experimental value of $Q(9/2)/Q(7/2) = 1.133 \pm 0.010$, one gets for the quadrupole moment at the $9/2^-$ excited state $Q(9/2) = (+\ 4.4 \pm 0.5)$b.

The ground state and the 6.2 keV state of ^{181}Ta have been classified as an intrinsic proton states with the Nilsson assignments $7/2^+[404]$ and $9/2^-[514]$, respectively [22]. In light of this one can pursue an elementary calculation for the change of the mean squared nuclear charge radius.

Nuclear Deformation

The relation between the intrinsic quadrupole moment Q_o, and the spectroscopic quadrupole moment Q is given by [30]

$$Q = Q_o \frac{3K^2 - I(I + 1)}{(I + 1)(2I + 3)} \quad . \tag{11}$$

Table 3. Summary of experimental results for the simultaneous fit of the ^{181}Ta in Re-metal velocity spectra shown in Fig. 8.

isomer shift IS	-(14.00±0.10)	mm/s
Q(9/2)/Q(7/2)	1.133±0.010	
e^2 q Q(7/2)	-(2.15±0.02)	10^{-6} eV
linewidth W	0.60±0.04	mm/s
effect A_{tot}	1.30±0.18%	spectrum (b)
	0.94±0.18%	spectrum (c)
Q(9/2)	+(4.4±0.5)	b
eq	-(5.5±0.5)	10^{17} V/cm^2

where K is the projection of I along the nuclear symmetry axis. For K = I,

$$Q = Q_o \frac{I(2I - 1)}{(I + 1)(2I + 3)} \quad . \tag{12}$$

With Q_o one associates a deformation parameter β, defined by

$$\beta = \frac{2}{3}\left(\frac{4\pi}{5}\right)^{1/2} \delta \quad ,$$

$$\text{with } Q_o = (4/5)Z\, R_o^2\, \delta(1 + (2/3)\delta),\ R_o = 1.2A^{1/3} \quad . \tag{13}$$

Thus, for the ^{181}Ta 7/2 ground state, Q(7/2) = 3.9±0.4b [29], therefore from equation (12), one gets

$$Q = (7/15)Q_o \text{ or } Q_o = (15/7)Q = +8.35b \quad . \tag{14}$$

From equation (13), one thus has

$$Q_o = 27\ \delta(1 + 2/3\ \delta) \quad . \tag{15}$$

Solving equation (15) using the result of (14), one then obtains

$$\delta = 0.26 \quad (\text{and } \delta = -1.76) \tag{16}$$

On the other hand, if one assumes the same deformation for the ground state (I = 7/2) and the excited state (I = 9/2), (the same Q_o) then from equation (12) it follows that

$$Q(9/2)/Q(7/2) = 1.169 \quad .$$

This is larger than the measured value of 1.133. Thus, one can write

$$\frac{Q_o(9/2)}{Q_o(7/2)} = \frac{1.133}{1.169} = 0.969 \quad .$$

From this one concludes that the excited state, I = 9/2, has a smaller deformation than the ground state. That is, $\Delta\langle r^2 \rangle$ is negative.

To get an estimate for $\Delta\langle r^2 \rangle$, one now has to relate it to $\Delta\delta$, which is the difference of the deformation parameter δ.

Letting $Q(9/2) - Q(7/2) = \Delta Q$ in equation (13), one gets $\Delta Q = (4/5)ZR_o^2\,(1 + 4/3\,\delta)\Delta\delta$.

Combining these two expression yields

$$\Delta\delta = \left[\frac{Q_o(9/2)}{Q_o(7/2)} - 1\right]\left[\frac{\delta(1 + \frac{2}{3}\delta)}{(1 + \frac{4}{3}\delta)}\right] \quad .$$

Using $\delta = 0.26$ from equation (16), in the above relation, one obtains

$$\Delta\delta = -\,(0.007 \pm 0.002)$$

$$\text{or} \quad \Delta\beta = -\,(0.0074 \pm 0.0023) \quad .$$

Now, to relate $\Delta\langle r^2 \rangle$ to $\Delta\beta$ one notes that

$$\langle r^2 \rangle = (3/5)R^2$$

$$\text{and} \quad R \sim R_o \left(\frac{5}{4\pi}\right)^{1/2} \beta$$

for incompressible nuclear matter [30]. Thus,

$$\Delta\langle r^2 \rangle = \frac{3}{2} R_o^2\, \beta\, \Delta\beta \quad . \tag{19}$$

Using the above values of β and $\Delta\beta$, the following estimate for $\Delta\langle r^2 \rangle$, the change of the mean squared nuclear charge radius, is derived:

$$\Delta\langle r^2 \rangle = -(4.5^{+1.1}_{-1.6}) \times 10^{-2}\ \mathrm{fm}^2 \ .$$

While the estimate is crude, the sign and magnitude seem to be in agreement with a different derivation based on isomer shift systematics, as is discussed in section VI.

V. ELECTRIC QUADRUPOLE INTERACTIONS OF ^{181}Ta IN HEXAGONAL TRANSITION METALS

Once the quadrupole moment ratio of the ground state and the 6.2 keV state, Q(9/2)/Q(7/2) (= 1.133±0.01), was obtained, other hosts for the ^{181}Ta impurities were used to determine the electric field gradient EFG [31]. In addition to the hexagonal metals used, (Re, Os, Ru, and Hf), the EFG was also observed in the tantalates, $LiTaO_3$ and $NaTaO_3$ [32]. In this section, only the hexagonal metal hosts will be discussed.

Source preparations for Os, Ru, and Hf hosts are detailed in section X. All measurements were done at room temperature using a single-line metal absorber. The resulting spectra are shown in Figs. 9, 10, and 11. Although the line widths are of the order of 100 times the natural line width of the 6.2 keV transition, the electric quadrupole splitting is well resolved. In analyzing these spectra η, the asymmetry parameter, was assumed to be zero, and for the cases of Os, Ru, and Hf, Q(9/2)/Q(7/2) was used as a fixed parameter (= 1.133±0.010). Thus, the EFG, the sign of the EFG, and the isomer shift were obtained. The dispersion term 2ξ(= 0.31±0.01) was also used as a fixed parameter. The results are summarized in Table 4.

To compare the results for the EFG with theoretical treatment, one can write the following relation for the total EFG, q:

$$q = q_{latt}(1 - \gamma_\infty) + q_{loc}(1 - R_Q) \quad , \qquad (20)$$

where γ_∞ and R_Q are the lattice and atomic Sternheimer factors, respectively. For ^{181}Ta, $\gamma_\infty \sim -60$ [33] and $R_Q \sim -0.2$ [34]. q_{latt} and q_{loc} are the

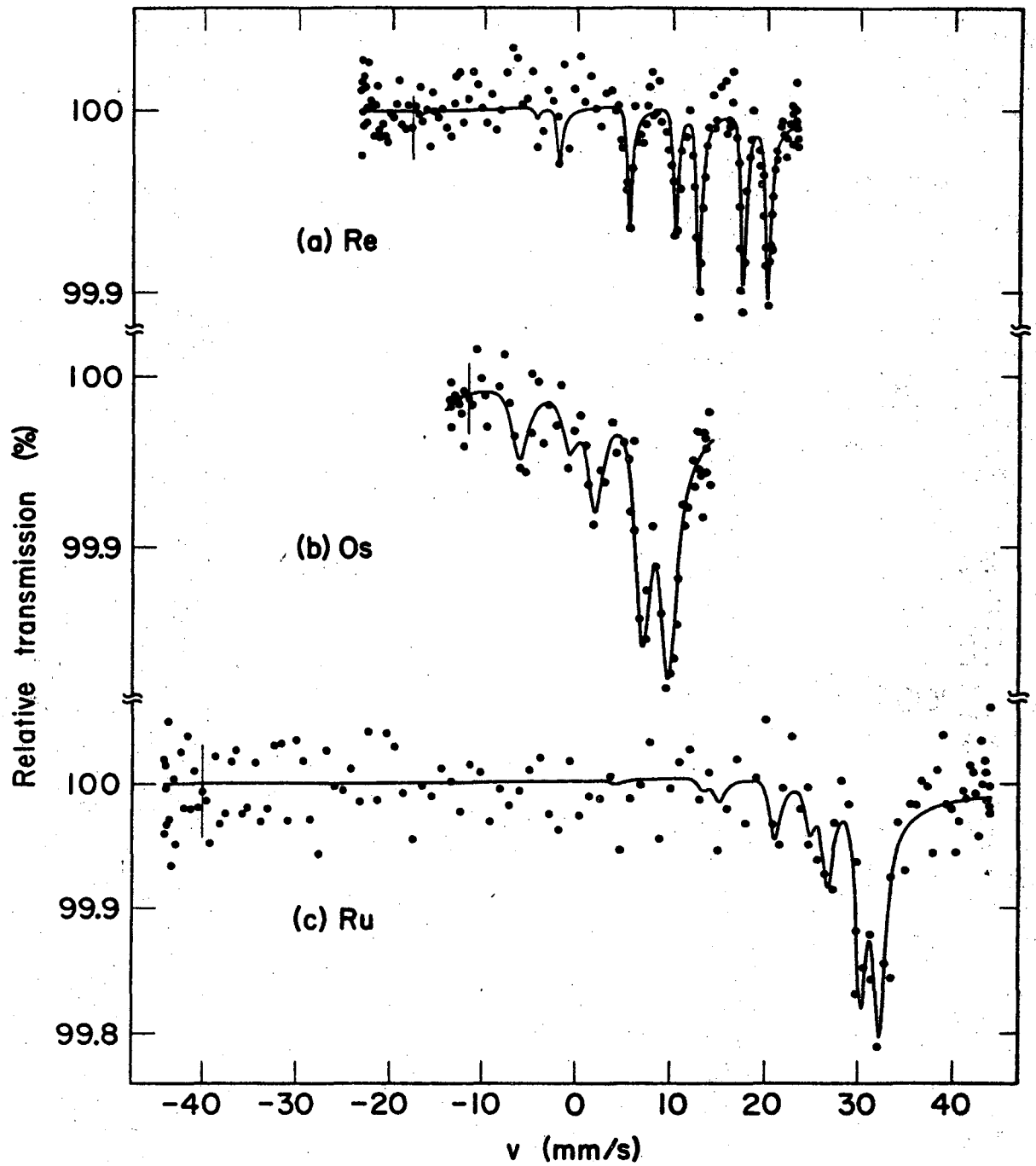

XBL722-2490

Fig. 9. Velocity spectra for ^{181}W(Re) (single crystal c axis perpendicular to observation direction), ^{181}W(Os) (polycrystal) and ^{181}W(Ru) (polycrystal) sources with a single-line Ta-metal absorber.

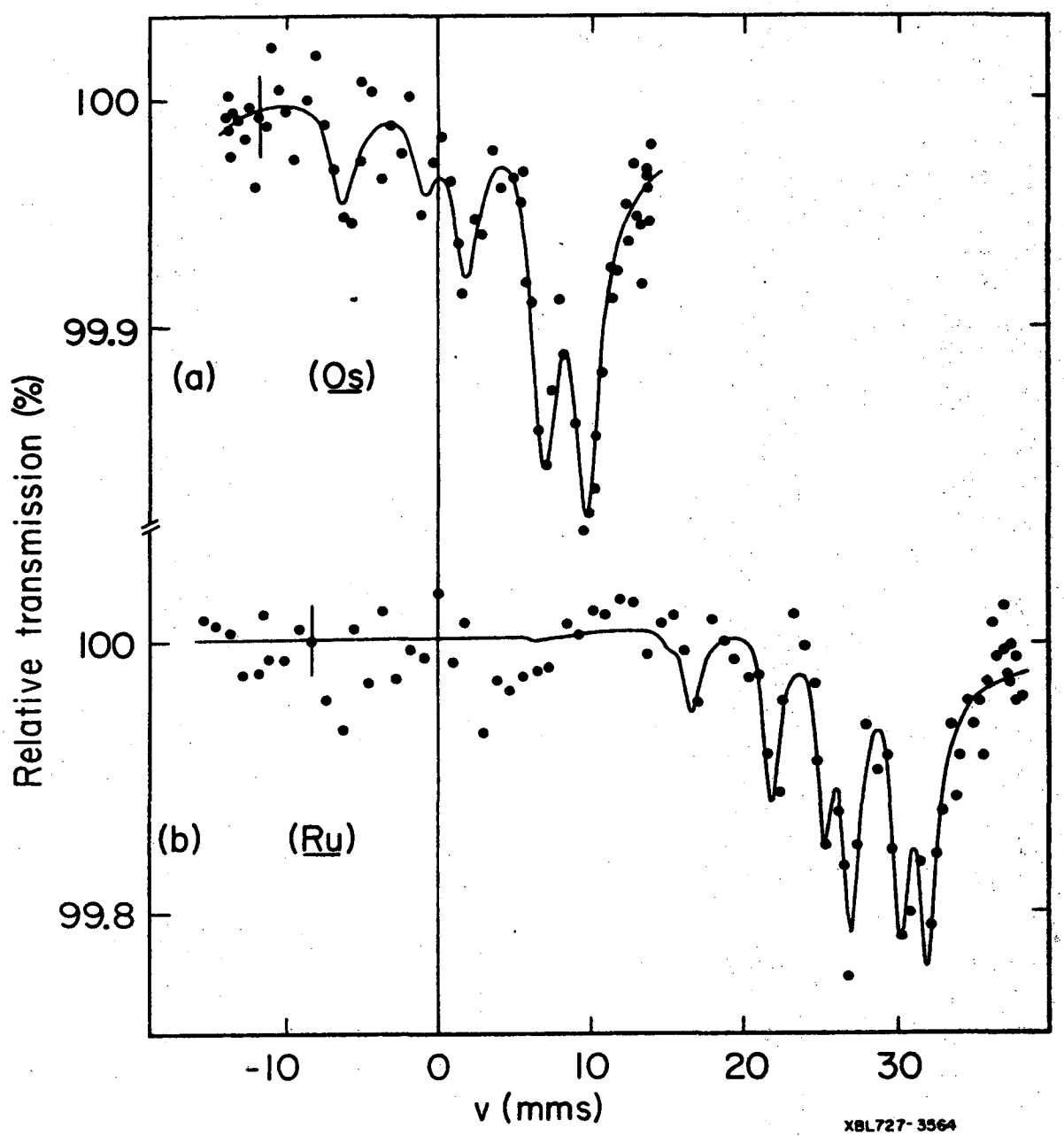

Fig. 10. Velocity spectra for ^{181}W(Os) (polycrystal), (same as Fig. 9(b)) and ^{181}W(Ru) single crystal (c axis perpendicular to observation direction) sources and a single-line Ta-metal absorber.

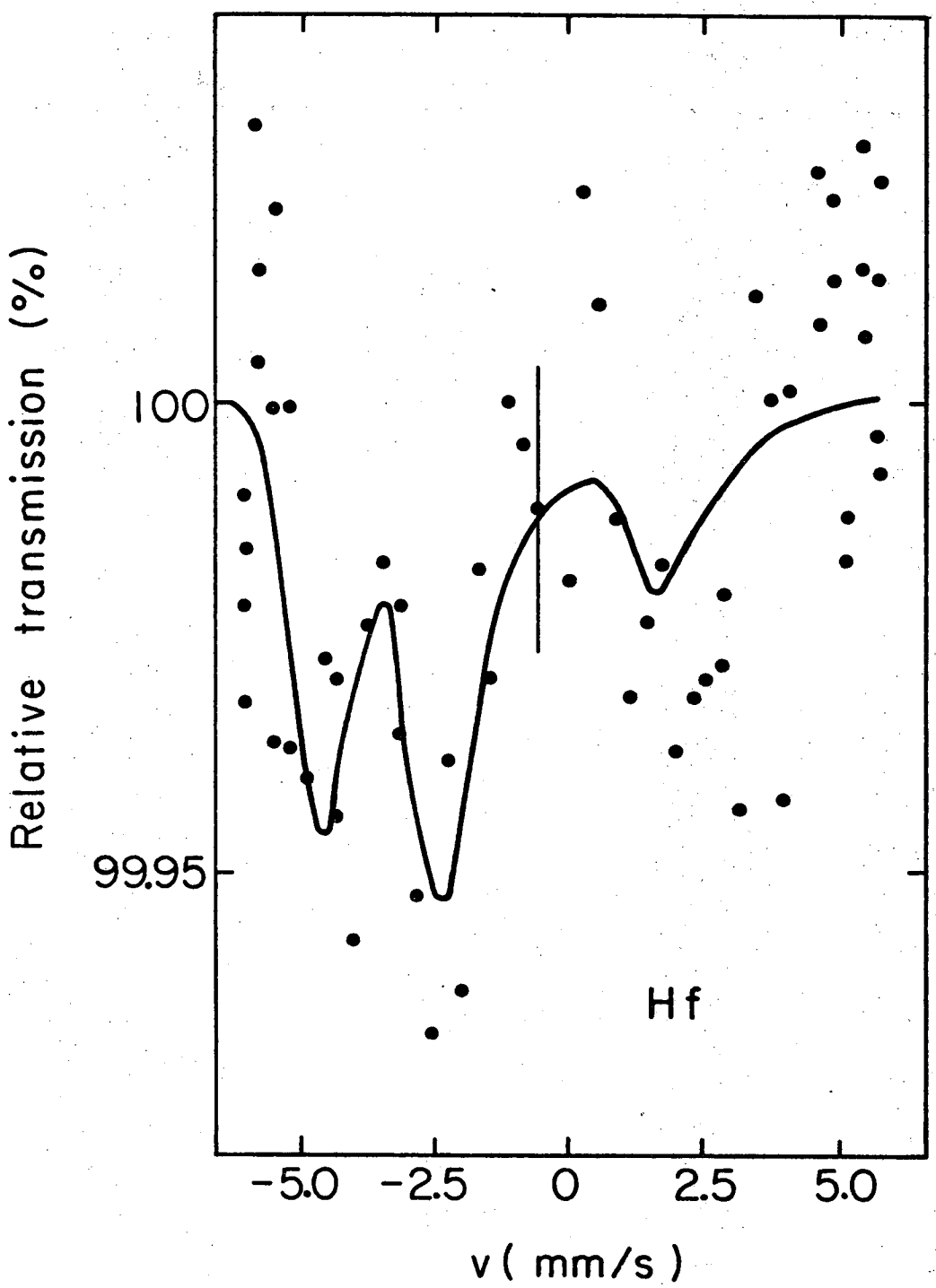

XBL 728-1560

Fig. 11. Velocity of ^{181}W(Hf) source and Ta-metal single absorber.

Table 4. Summary of experimental results for ^{181}Ta impurities in transition metals.

host	$e^2qQ(7/2)$ (10^{-6} eV)	eq (10^{17} V/cm^2)	IS (mm/s)	W (mm/s)
Re	-2.15±0.02	-5.5±0.5	-14.0±0.1	0.60±0.04
Os	-2.35±0.04	-6.0±0.7	-2.9±0.2	1.8±0.2
Hf	+1.83±0.10	+4.7±0.7	-0.6±0.3	1.6±0.4
Ru	-1.56±0.04	-4.0±0.5	-27.6±0.3	1.3±0.2

lattice and local contribution to the EFG, respectively. Watson et al. [35] account for the q_{loc} contribution by the localized change around the central atom and the non-uniform distribution of the conduction electrons. The latter effect they consider as a major contribution, especially in cases where the density of states is high at the Fermi energy. They then predict an "overshielding effect", so that one can write $q_{loc} = r \cdot q_{latt}$. Equation (20) can now be written as

$$q = q_{latt}[(1 - \gamma_\infty) + r(1 - R_Q)] \quad . \tag{21}$$

One can now calculate the q_{latt} according to DeWette's tables [36]. The results for eq/Z (point ion model) are tabulate in Table 5. Z is the number of conduction electrons in the conduction band, and is 4, 7, 8, and 4 for Hf, Re, Os, and Ru, respectively. Using equation (21) and equating it to the experimental values for the EFG, one gets the "overshielding" factors r shown in Table 5. These compare with the theoretical values of Watson et al. of -100, -55, and -7 for Re, Os, and Ru, respectively. The agreement with Re and Os is not bad. The positive sign for the EFG for Hf indicates that in this case the lattice contribution plays an essential role.

$$q = q_{latt}[(1 - \gamma_\infty) + r(1 - R_Q)]$$

$$\gamma_\infty \sim -60 \quad ; \quad R_Q \sim -0.2$$

This is indicated by TDPAC studies of the 482 keV state of ^{181}Ta [37], where the EFG was measured as a function of temperature.

Table 5. Comparison of experimental EFG with point ion model (after DeWette [36]), and the deduction of the "overshielding" parameter (according to Watson *et al.* [35]).

	eq 10^{17}[V/cm^2] experimental	eq/Z 10^{14}[V/cm^2] point ion model	r
Hf	+4.7 (7)	+10.05	+ 36
Re	-5.5 (5)	+ 5.97	-160
Os	-6.0 (7)	+17.4	- 85
Ru	-4.1 (5)	+16.41	- 75

Finally, in Table 6 the EFG in hexagonal transition metals is compared with other results utilizing different techniques and probe nuclei. The Mössbauer technique with the 6.2 keV has the advantage that the sign is measured as well, and at room temperature. The 482 keV level of ^{181}Ta with TDPAC method is also a powerful method, once the sign of the EFG is known. Studies of the EFG as a function of temperature are currently underway [38], but they are beyond the scope of this work.

Table 6. Comparison of electric field gradients, eq, in hexagonal transition metals between present results and other methods. NAR (Nuclear Acoustic Resonance), NSH (Nuclear Specific Heat), M (Mössbauer), TDPAC (Time Differentiated Perturbed Angular Correlation).

host	probe nucleus	T [K]	eq 10^{17}[V/cm^2]	method
Re	^{181}Ta (6.2 keV)	300	-(5.5±0.5)	present result
Re	^{185}Re, ^{187}Re	4.2	-(4.9±1.9)	NAR[39],NSH[40]
Re	^{186}Os, ^{188}Os	4.2	-(3.3±0.6)	M[41]
Hf	^{181}Ta (6.2 keV)	300	+(4.7±0.7)	present result
Hf	^{178}Hf	4.2	+(9.5±0.4)	M[42]
Hf	^{181}Ta (482 keV)	300	(5.5±0.3)	TDPAC[37]
Os	^{181}Ta (6.2 keV)	300	-(6.0±0.7)	present result
Ru	^{181}Ta (6.2 keV)	300	-(4.1±0.5)	present result

VI. ISOMER SHIFTS

The unique features of the 6.2 keV γ resonance among all other Mössbauer transitions are most clearly exhibited by the isomer shift results. Isomer shifts were observed for ^{181}Ta impurities in 5d, 4d, and 3d transition metals, and for Ta compounds, and covered a range of 110 mm/s. This range corresponds to 17,000 times the natural line width ($\Gamma_o = 2\hbar/\tau = 6.436\ 10^{-3}$ mm/s), or 1,600 times the minimum experimental line width obtained up to now [43].

^{181}W activity was diffused into transition metals hosts for sources. These were measured with a Ta-metal absorber. The compounds, on the other hand, were all used as absorbers and were measured with a ^{181}W(W) source. Details of the preparation of these are discussed in section X.

One precaution had to be taken in measurement of cases where the isomer shift ratio to the line width was quite large (e.g. Nb, Mo, and Ni). The solid angle of source-absorber-counter arrangement had to be kept small in order to avoid excessive geometrical broadening and consequently a decrease of the observed resonance effect. For example, for ^{181}W(Mo), where the isomer shift is 22.5 mm/s, even a small solid angle of $4\pi/500$ corresponds to a spread of 0.10 mm/s.

Experimental velocity spectra for all the single line cases are shown in Figs. 12, 13, and 14. (The cases of split spectra are shown in sections IV, V, and VIII.) The isomer-shift results are compiled in Table 7, and are graphically represented in Fig. 15.

The experimental line width ranged from 17 times the natural line width for the W source to 1,200 times for the V source. And the

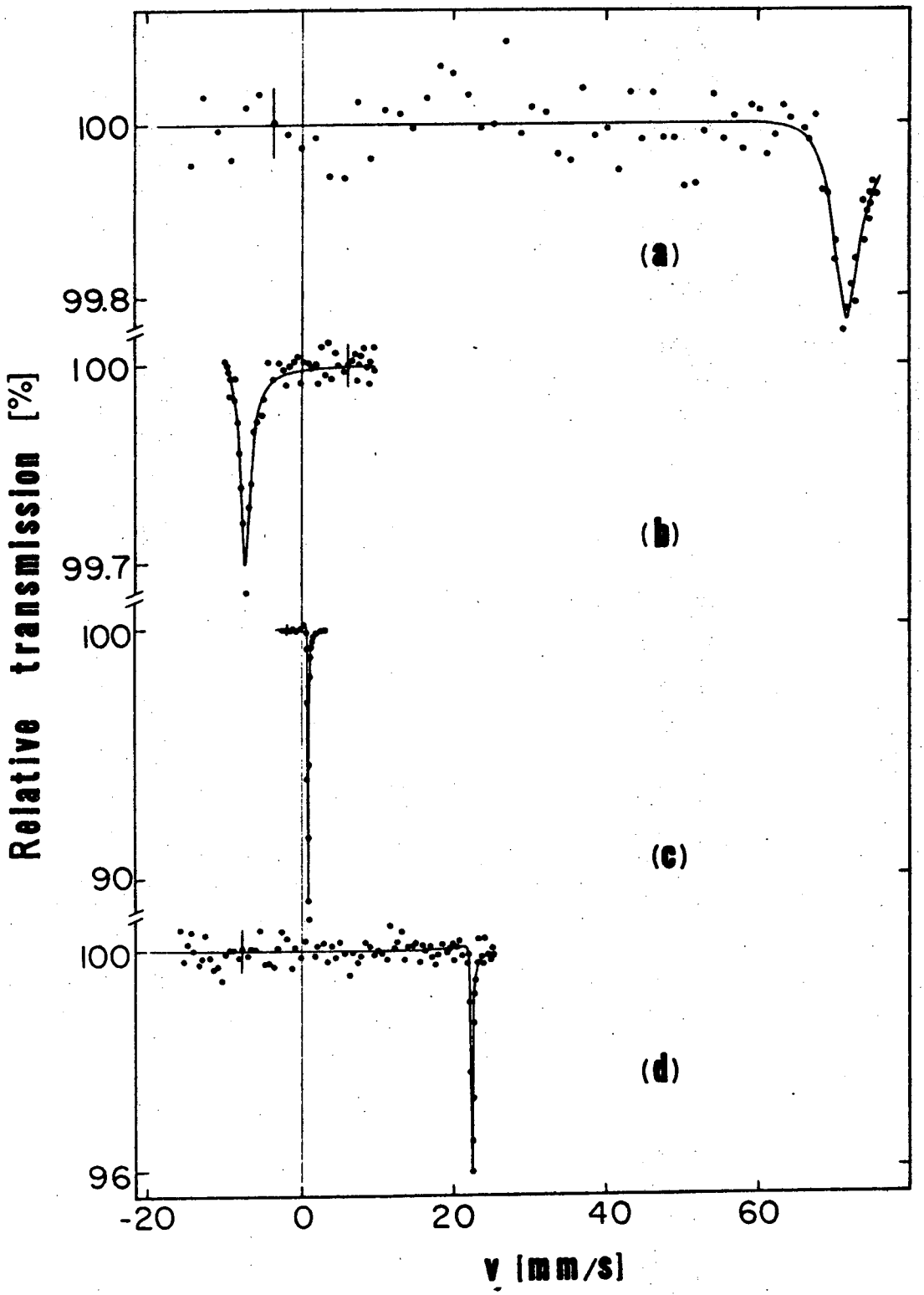

XBL721-2156

Fig. 12. Velocity spectrum of (a) TaC and (b) $KTaO_3$ absorbers using a $^{181}W(\underline{W})$ source. In (c) and (d) the spectrum are of $^{181}W(\underline{W})$ and $^{181}W(\underline{Mo})$ sources analyzed with a Ta-metal absorber.

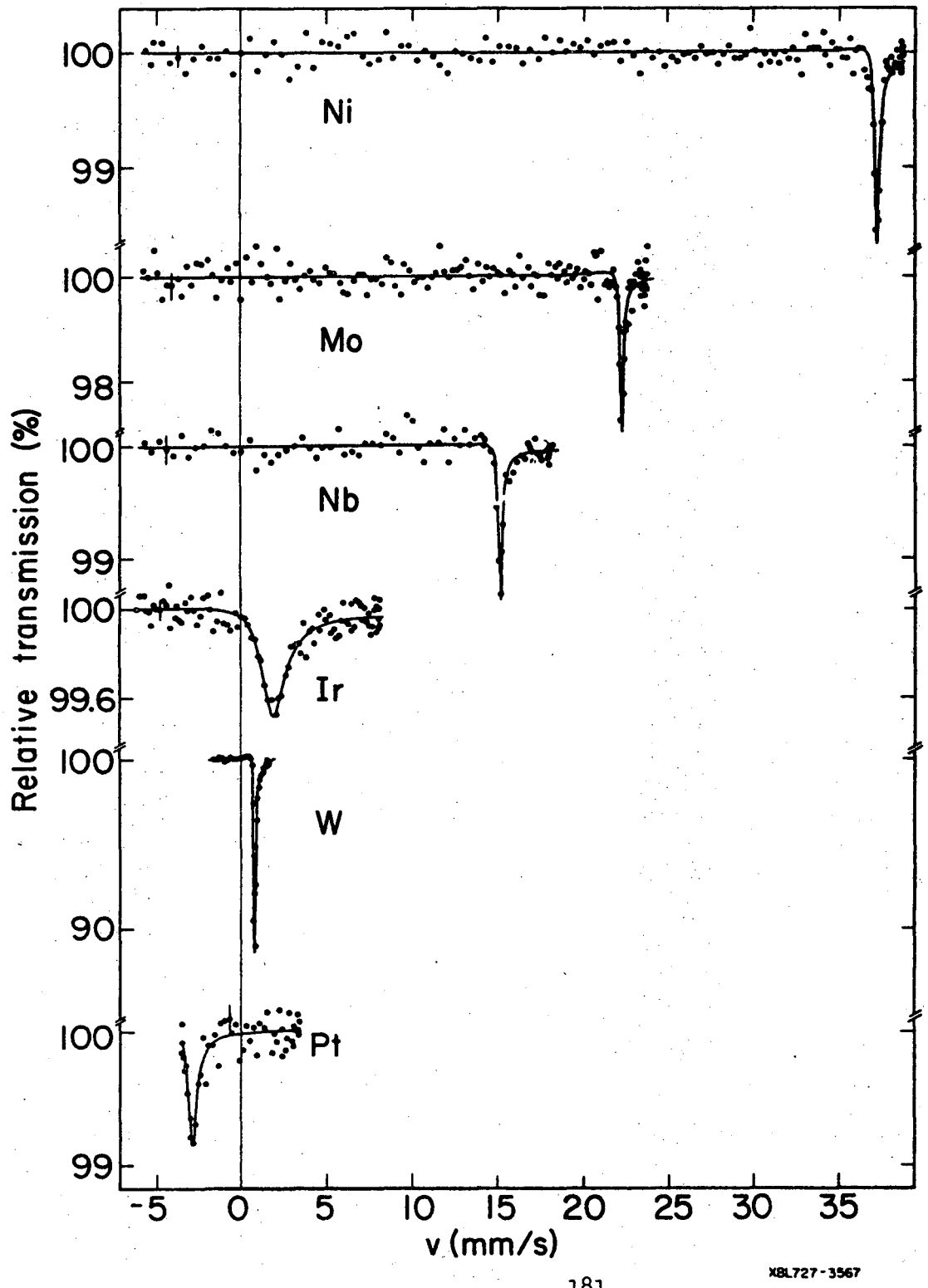

Fig. 13. Velocity spectra for sources of ^{181}W diffused hosts, analyzed with a Ta metal absorber. Except for the Ni case, measurements were made at room temperature. The Ni source was measured at 412°C (see section VII and IX).

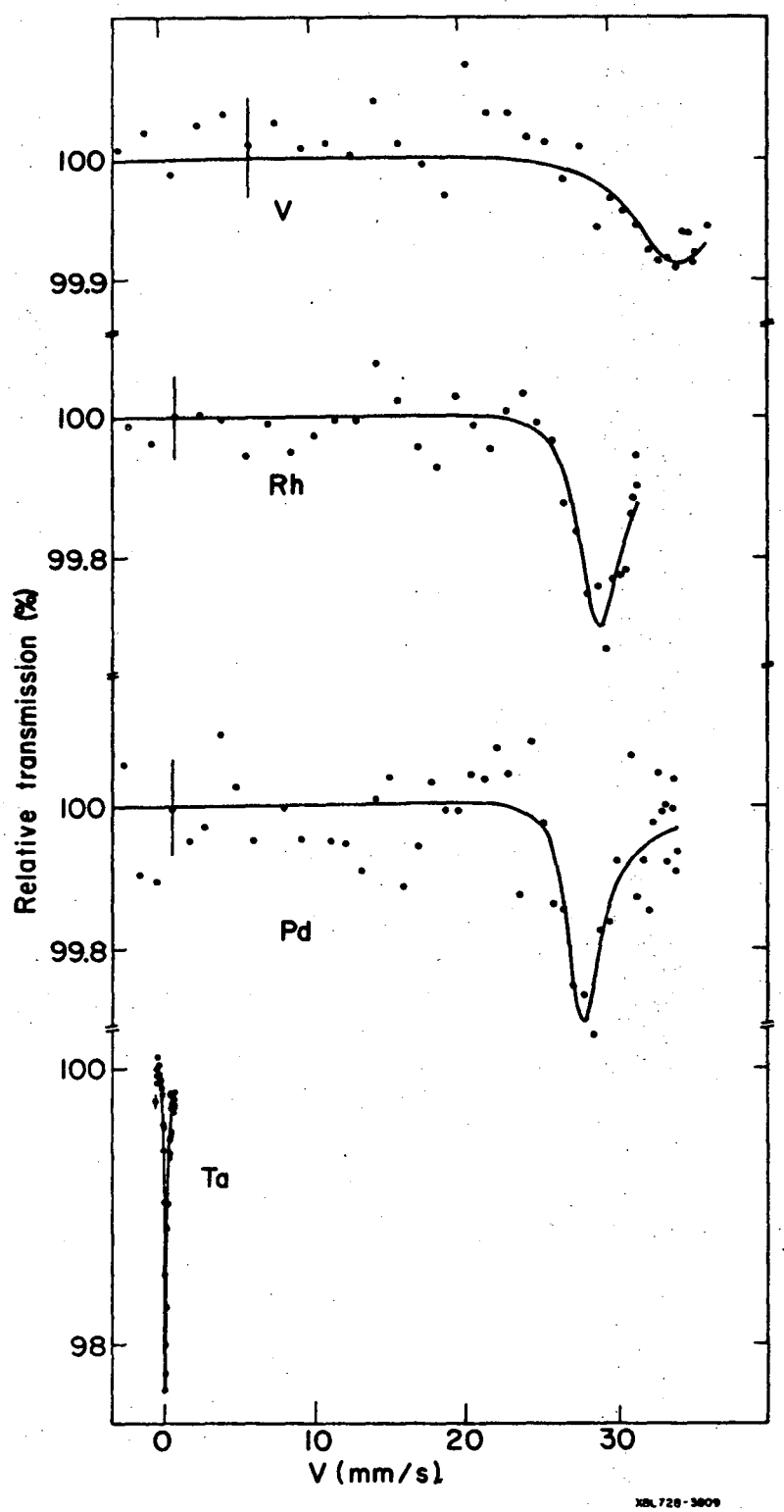

Fig. 14. Velocity spectra for the "wide" line cases of V, Rh, and Pd contrasted with the ^{181}(Ta) source. Again, all were analyzed at room temperature with a Ta-metal absorber.

Table 7. Tabulation of the isomer shift results. The isomer shifts are given relative to Ta-metal, with source and absorber at room temperature. (The value of Ni was extrapolated from the temperature dependence of the isomer shift in the Ni lattice (see section VI).)

Source Lattice	IS (mm/s)	W(FWHM) (mm/s)	Effect (%)
V	-33.6±0.7	7.7±2.6	0.1
Ni	-39.5±0.2	0.50±0.08	1.6
Nb	-15.28±0.10	0.15±0.06	1.4
Mo	-22.50±0.10	0.22±0.03	3.0
Ru	-27.50±0.30	1.3±0.2	0.7
Rh	-28.80±0.25	3.4±0.5	0.3
Pd	-27.55±0.25	2.7±0.6	0.3
Hf	-0.60±0.30	1.6±0.4	0.2
Ta	-0.075±0.004	0.184±0.006	2.4
W	-0.860±0.008	0.112±0.002	11.3
Re	-14.00±0.10	0.60±0.04	1.3
Os	-2.35±0.04	1.8±0.2	0.8
Ir	-1.84±0.04	1.60±0.14	0.5
Pt	+2.66±0.04	0.30±0.08	0.9
Absorbers			
$LiTaO_3$	-24.04±0.30	1.6±0.2	0.9
$NaTaO_3$	-13.26±0.30	1.0±0.2	0.9
$KTaO_3$	-8.11±0.15	1.5±0.2	0.3
TaC	+70.8±0.5	2.4±0.4	0.2

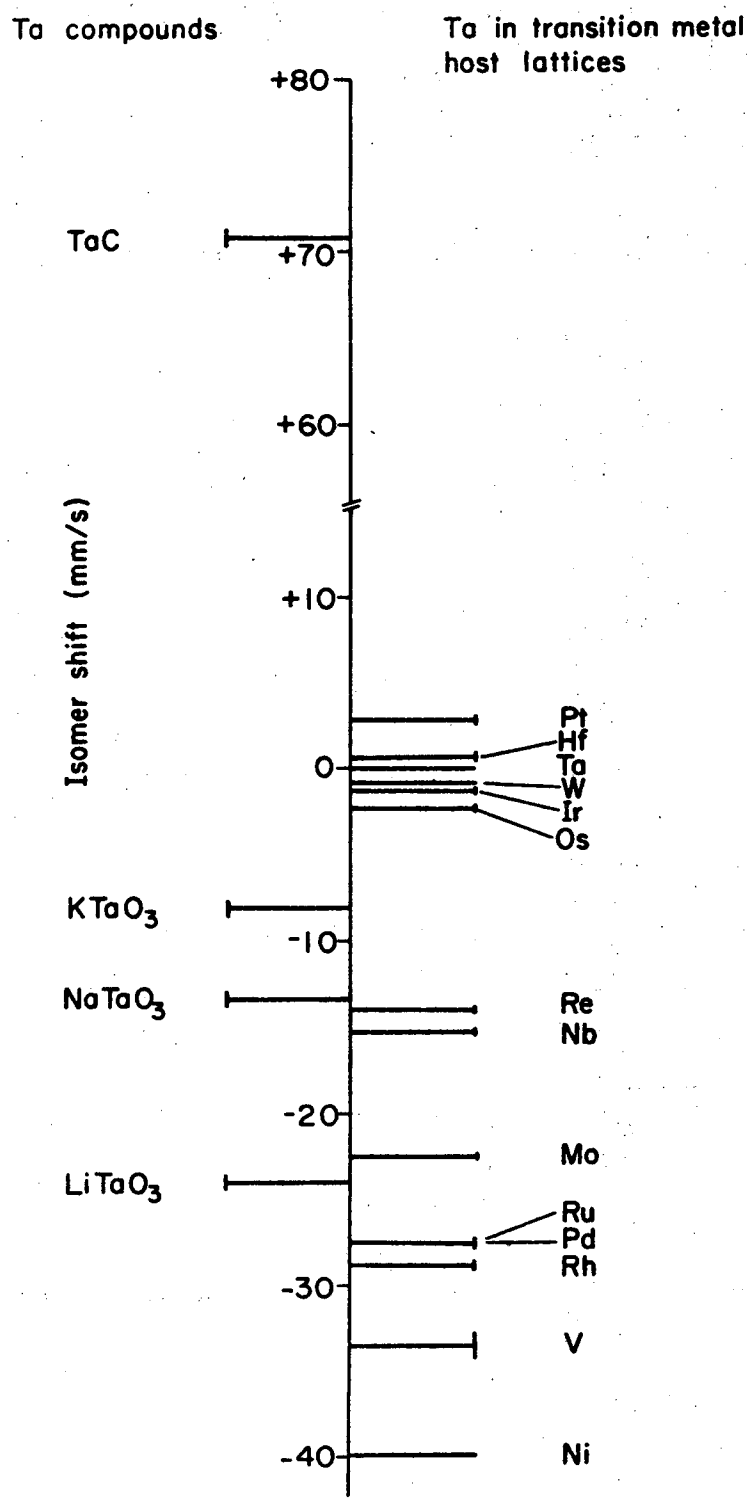

Fig. 15. Graphical representation of isomer shift of Ta 6.2 keV ray of Ta. While the whole range is about 110 mm/s, the range in the transition metals alone is 43 mm/s.

size of the uncorrected effect exhibited similar behavior: from 11.3% for W to 0.1% for V. The narrowest line widths in the 4 and 5d hosts were observed for those metals which are continuously miscible with Ta metal. The best experimental line shifts to line width ratio are the cases of Mo, Nb, and Ni, even though the line widths are up to 77 times the natural line width (Ni case). (Experimental difficulties with sources and observation of effects are discussed in section X.)

Systematics of the Isomer Shifts and an Estimate for $\Delta\langle r^2 \rangle$

In Fig. 16 the isomer shifts data for the transition metals hosts is plotted as a function of the number of the outer electrons for the 5d, 4d, and 3d series. As one can see, an interesting systematic behavior is exhibited. The isomer shift is "highest" for the 5d, "lower" for the 4d, and "lowest" for the 3d series. In other words, the transition energy decreases as one moves from a 5d to a 4d and further to a 3d host element in a vertical column of the periodic system.

Similar systematic behavior has been observed for the isomer shifts of the 14.4 keV γ transition of ^{57}Fe [44], the 77 keV γ transition of ^{197}Au, and the 90 keV γ transition of ^{99}Ru [45]. (These results are summarized in Appendix III.) For these cases the sign of the changes of the mean-squared-nuclear-charge-radius, $\Delta\langle r^2 \rangle$, is known [46]. Thus, using the relation of equation (5) page 5, one can derive from the isomer shifts systematics the behavior of the changes of the total electronic density, $\Delta|\psi_o|^2$, at the impurity nucleus. For impurities of ^{57}Fe, ^{197}Au, and ^{77}Ru in the transition metals, it then follows that the electron density at the probe nucleus increases when one proceeds from a 5d to a

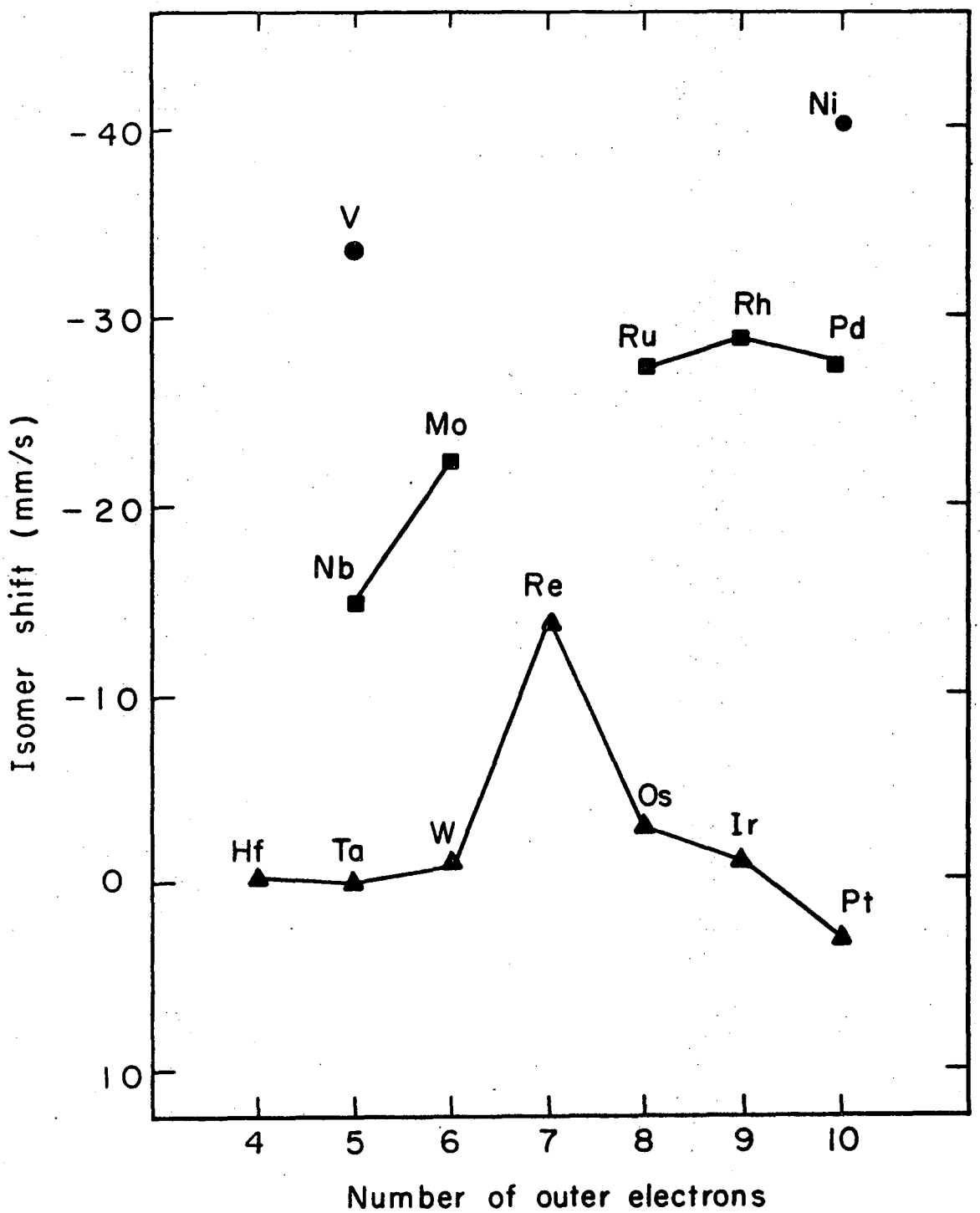

Fig. 16. Systematics of the isomer shifts for ^{181}Ta impurities in the transition metal hosts.

4d and finally to a 3d host metal in a vertical column. If one then assumes the same above correlation for the electron density at ^{181}Ta impurities, then one can conclude that $\Delta\langle r^2 \rangle$ is negative for the 6.2 keV transition; the 6.2 keV transition energy decreases in a vertical column as one goes from 5d to 4d and to a 3d host (Fig. 16).

Having established that the sign is negative, one can now proceed to get an estimate for the magnitude of $\Delta\langle r^2 \rangle$ by using $\Delta|\psi_o|^2$ calculated for other 5d impurities. In the case of the 99 keV Mössbauer transition of ^{193}Ir, which follows the isomer shifts systematics mentioned above [47], the isomer shifts of ^{193}Ir(Ni) and ^{193}Ir(Pt) give a $\Delta|\psi_o|^2$ $(= |\psi_o|^2(\mathrm{Ni}) - |\psi_o|^2(\mathrm{Pt}))$ of the order of 3.5×10^{26} cm^{-3}. Similarly, from the ^{197}Au isomer shifts measurements of ^{197}Au(Ni) and ^{197}Au(Pt) [45] and the value of $\Delta\langle r^2 \rangle = 1.5 \times 10^{-2}$ fm^2 for ^{197}Au [48], a value of $\Delta|\psi_o|^2 = 2.7 \times 10^{26}$ for ^{197}Au is derived.

One can then assume, after relativistic corrections [11] an average value for ^{181}Ta of 2.5×10^{26} cm^{-3} for $\Delta|\psi_o|^2$ $(= |\psi_o|^2(\mathrm{Ni}) - |\psi_o|^2(\mathrm{Pt}))$. Using, now, the isomer shift difference of 42 mm/s for ^{181}Ta in Ni and Pt, a value of the change of the mean square nuclear charge radius for ^{181}Ta is obtained:

$$\Delta\langle r^2 \rangle \sim -1.6 \times 10^{-2} \text{ fm}^2 \quad .$$

Again, this is only a rough estimate, which agrees with the earlier derivation in section IV in order of magnitude and sign.

VII. TEMPERATURE DEPENDENCE OF THE ISOMER SHIFTS IN TRANSITION METALS

One of the most subtle effects of the 6.2 keV transition of ^{181}Ta is the variation in line position for ^{181}Ta impurities in transition metals as a function of temperature. The interesting result is that temperature dependence is not the usual thermal red shift usually observed for ^{57}Fe and ^{119}Sn [49,50]. Rather, it is a result of hyperfine interaction effects. In fact, for the case of ^{181}Ta(Ni) the temperature shift of the isomer shift is -33 times the thermal red shift expected for a Debye solid at high temperature, and is equivalent to a shift of 2.3 natural line widths per degree.

The host transition metals studied were Ta, W, Ir, Pt, Mo, Pd, and Ni. The experimental set-up is shown in Fig. 17. The sources were heated from 300 K (room temperature) to 1100 K, while the Ta-metal absorber was left at room temperature.

Some of the experimental results are shown in Fig. 18. As can be seen, the data can well be described by a linear relationship between the line shift (S) and the temperature. The solid curves are least square fits of straight lines.

The thermal red shift, or the second order Doppler shift (SODS), is given at high temperature for a Debye solid by $-3k/2Mc$ in cm/s [6]. For the 6.2 keV γ transition of ^{181}Ta it is -2.299×10^{-4} mm/s per degree, and it is plotted in Fig. 18(e) as a comparison to experimental results. In the case of ^{57}Fe, Pound et al. [51,49] found from temperature and pressure effects that only 8% of the temperature shift was due to lattice thermal expansion; the main shift being the SODS. Recent experiments for β-tin by Rothberg [52] also showed that the main shift was due to SODS.

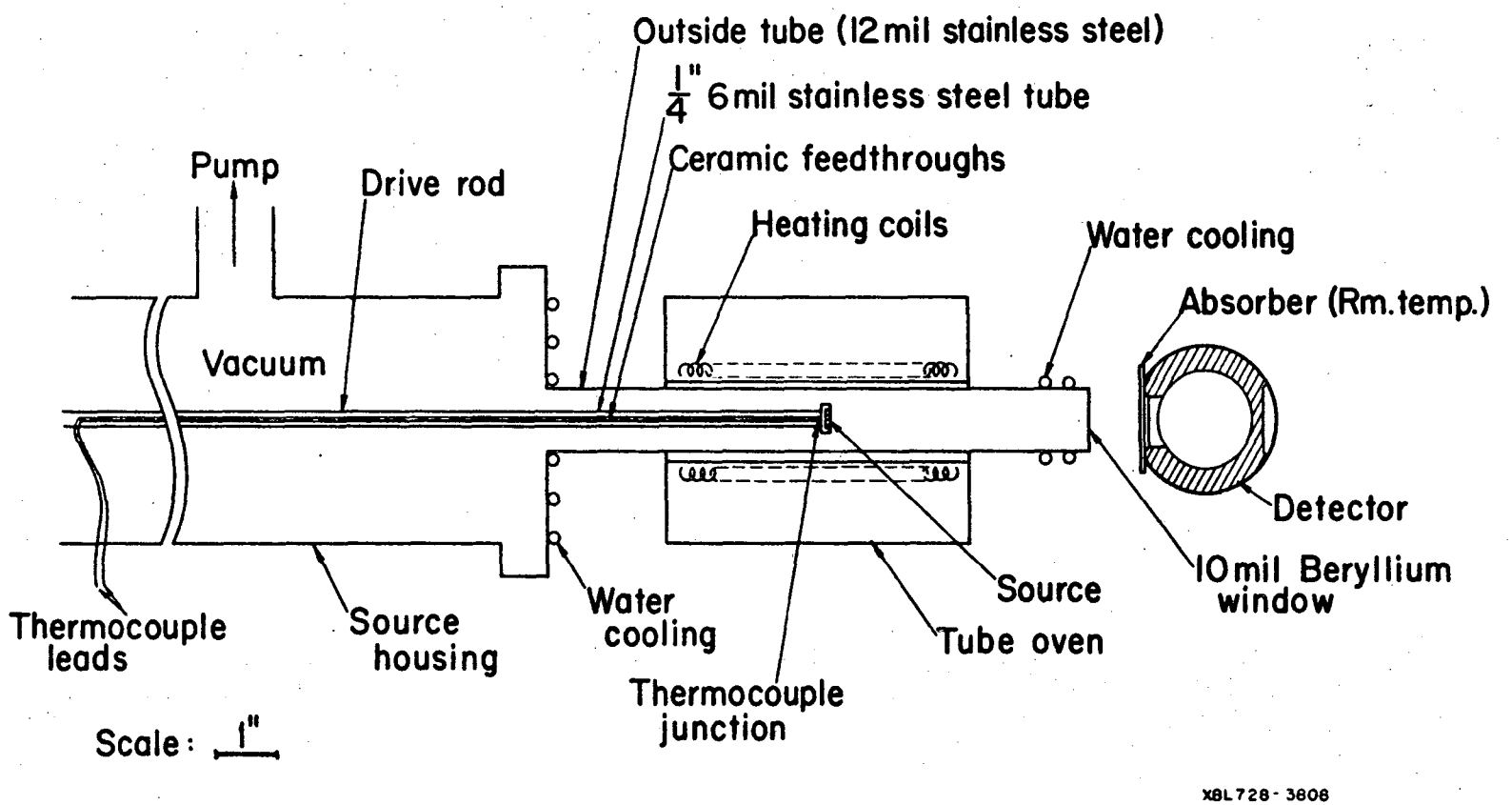

Fig. 17. Experimental arrangement for temperature studies (300 K to 1,100 K). The Pt-Pt/Rh thermocouple was directly in contact with the source metal discs as shown.

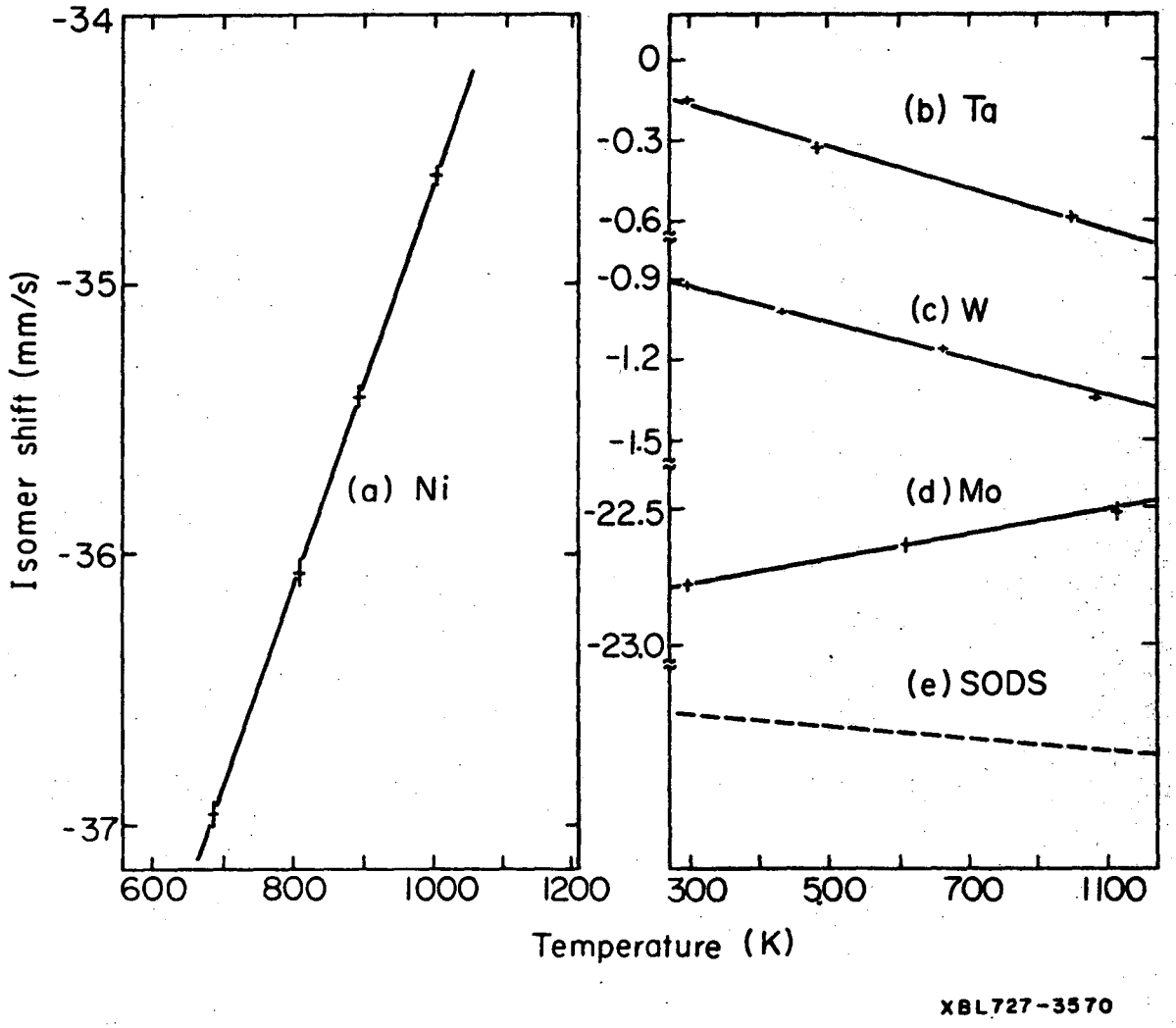

Fig. 18. Relative temperature dependence of line shifts for sources of ^{181}W diffused into (a) Ni, (b) Ta, (c) W, and (d) Mo. In (e) the expected second order Doppler shift for ^{181}Ta is also plotted. All curves are plotted with the same scale on both axis.

For the experimentally observed temperature variation of the line position S one can write [51,52]:

$$\left(\frac{\partial S}{\partial T}\right)_P = \left(\frac{\partial S_{SODS}}{\partial T}\right)_P + \left(\frac{\partial S_{IS}}{\partial T}\right)_V + \left(\frac{\partial S_{IS}}{\partial \ \ell nV}\right)_T \left(\frac{\partial \ \ell nV}{\partial T}\right)_P \tag{22}$$

The first term represents the second order Doppler shifts. The second term is then the explicit temperature dependence of the isomer shift at constant volume. This is due to electron density changes caused by the effects of electron-phonon interaction on the electronic state of the conduction electrons. The third term describes the volume dependence of the isomer shift created by thermal expansion.

The experimental data are summarized in Table 8 in the column headed $\left(\frac{\partial S}{\partial T}\right)_P^{\dagger}$. These values are then corrected for the thermal red shift (SODS) to yield the values for the isobaric temperature dependence of the isomer shift, $\left(\frac{\partial S_{IS}}{\partial T}\right)_P$. One notes that for Ni and Mo and γ ray energy increases with increasing temperatures, while for Ta, W, Ir, Pt, and Pd, the γ ray energy decreases.

The isobaric temperature dependence of the isomer shift measured here can not as yet be separated into an explicit temperature dependent part, $\left(\frac{\partial S_{IS}}{\partial T}\right)_V$, and volume dependent part, $\left(\frac{\partial S_{IS}}{\partial \ \ell nV}\right)_T \left(\frac{\partial \ \ell nV}{\partial T}\right)_P$. However, pressure experiments on host lattices can be performed to yield values of $\frac{\partial S_{IS}}{\partial \ \ell nV}_T$. These experiments are outside the scope of this work. However, an estimate of the magnitude can be made.

Measurements for ^{57}Fe impurities in host lattices of the transition metals [54] show that values of $\left(\frac{\partial S_{IS}}{\partial \ \ell nV}\right)_T$ lead to a definite systematic

---

†Of the measurements presented here, the values for W and Ta agree with the earlier results of Taylor et al. [53].

Table 8. Isobaric temperature variation of transition energy of the 6.2 keV γ rays, $\left(\frac{\partial S}{\partial T}\right)_P$, for ^{181}Ta impurities in transition metal hosts (column 2). In column 3 the derived fraction due to isomer shift, $\left(\frac{\partial S_{IS}}{\partial T}\right)_P$, is given, and in column 4 the isobaric thermal expansion coefficients extracted from x-ray data for the present temperature region (0-800°C) is also tabulated.

host metal	$\left(\frac{\partial S}{\partial T}\right)_P$ (10^{-4} mm/s deg^{-1})	$\left(\frac{\partial S_{IS}}{\partial T}\right)_P$ (10^{-4} mm/s deg^{-1})	$\left(\frac{\partial \ell nV}{\partial T}\right)_P$ (10^{-5} deg^{-1})
Ni	73.2±3.5	75.5±3.5	5.15
Mo	3.6±0.6	5.9±0.5	1.67
Pd	-16.7±7.0	-14.4±7.0	~ 4.0
Ta	-8.0±0.5	-5.7±0.5	2.03
W	-7.1±0.2	-4.8±0.2	1.42
Ir	-7.2±4.1	4.9±4.1	~ 2.0
Pt	-17.6±0.9	-15.3±0.9	2.92

increase with decreasing isomer shift or increasing $|\psi_o|^2$. In other words, a simple scaling of $|\psi_o|^2$ to volume changes can be approximated, taking into account opposite contributions of s- and d-like conduction electrons. If one then extends this scaling to $^{181}Ta^{\dagger}$ in Ni, using for Ni $\Delta V/V \sim 5.15 \times 10^{-4}$ deg^{-1}, and $|\psi_{6_s}|^2$, the s density at the Ta nucleus, $\sim 2 \times 10^{27}$ cm^{-3} [56], then $\Delta|\psi_o|^2$ corresponding to this volume change is $\sim 1.03 \times 10^{23}$ cm^{-3}.

Using $\Delta\langle r^2 \rangle = 1.6 \times 10^{-2}$ fm^2 and the relation of isomer shift to $\Delta|\psi_o|^2$ in equation (6), page 5, one gets

$$\left(\frac{\partial S_{IS}}{\partial \ \ell nV}\right)_T \left(\frac{\partial \ \ell nV}{\partial T}\right)_P \sim 170 \times 10^{-4} \text{ mm/s deg}^{-1}$$

This is more than twice as large as the experimental value of the isobaric temperature dependence.

On the other hand, the explicit temperature dependence, $\left(\frac{\partial S_{IS}}{\partial T}\right)_V$, is expected to be negative for ^{181}Ta. With increasing temperature the electron-phonon interaction should cause a small d → s electron transfer, thus increasing the electron density linearly with temperature [57,52]. Thus, the above two effects seem to be of the same order in light of the observed isobaric temperature variation of the isomer shift, being positive for Ni and Mo and negative for Ta, W, Ir, Pt, and Pd. Furthermore, one can then expect the volume shift to increase with decreasing isomer shift (5d to 3d) and to be dominating for the overall temperature shifts

---

†See also Ref. 55 for pressure experiments of ^{197}Au, which also support the assumptions here.

of Ni and Mo. For the 5d elements then, the dependence is dominated by the explicit temperature variation.

Clearly, the above arguments are only comments on general possible trends; the Pd case is hard to account for.

VIII. Ta COMPOUNDS

Mössbauer absorption effects were observed for TaC and the tantalates of Li, Na, and K. The preparation techniques are discussed in section X.

TaC is more a metal-like compound. The question whether it exhibits metal-like or covalent bonding is not very clear [58]. However, the fact that a resonance for ^{181}Ta was observed in this compound, indicates the value of a systematic study of other metal-like tantalum compounds, namely TaN, TaS, and TaS_2. The problem is not simple, as one can note that even though the isomer shift for TaC is impressively large, the line width is relatively wide (400 times the natural line width) and the effect is 0.2% for the single line case of TaC.

Ta compounds exist in three formal oxidation states (III, IV, and V) of which the pentavalent state is the most stable. The compounds studied here were the pentavalent tantalates, whose isomer shifts are of the same order of magnitude as those of the metals. If one then compares systematics of isomer shifts versus valence states for ^{57}Fe, ^{99}Ru, ^{193}Ir, and ^{189}Os [59], one then notes that the isomer shifts order themselves according to the increasing or decreasing valence states of the compounds. One can then surmise that isomer shift for the IV- and III-valent Ta compounds would be outside of the isomer shift range observed up to now. The question of how far outside the present range the III and IV valent isomer shift are, can be partially answered by the isomer shift of TaC. If TaC, the metal-like compound, is more like a IV- rather than V-valent compound then the isomer shift of III and IV valent could be anticipated to be spaced in the order of 100 mm/s from the V-valent compounds.

The Tantalates

Velocity spectra of TaO_3, $NaTaO_3$, and $KTaO_3$ are shown in Figs. 19 and 20. In the $LiTaO_3$ and $NaTaO_3$ cases, hyperfine splitting by the EFG is observed. $KTaO_3$, which is cubic, exhibits only a single line spectrum. All velocity spectra were taken at room temperature. The $LiTaO_3$ is a special case in that the absorber, prepared from fine crystal powder, actually became oriented to a high degree, with the c axis perpendicular to the plane. This is very clearly exhibited in Fig. 19, where the only difference between the spectra (b) and (c) is a tilt of 45° of the absorber in (c). This, incidently, was necessary for the determination of the sign of the EFG.

The results of a least-square fit are tabulated in Table 9. Both the quadrupole moment ratio and the dispersion term were kept constant. The EFG was assumed to be axially symmetric. This is at least true for $LiTaO_3$.

The isomer shifts exhibit a definite systematic behavior, namely an increase in the electron density at the Ta nucleus as one proceeds from K to Na and further to Li tantalate. Here one uses the results of section V, where it was established that $\Delta\langle r^2 \rangle$ is negative. In Table 10 the EFG at the Ta site in $LiTaO_3$ is compared with values measured by NMR in $LiNbO_3$ [60]. The NMR results for the EFG at the Li site were obtained for both $LiTaO_3$ and $LiNbO_3$, but for the Ta/Nb site, only the Nb site was determined. The probe nucleus there was ^{93}Nb.

Further studies of the tantalates with the 6.2 keV transition could be of interest, mostly in regards to their ferroelectric properties.

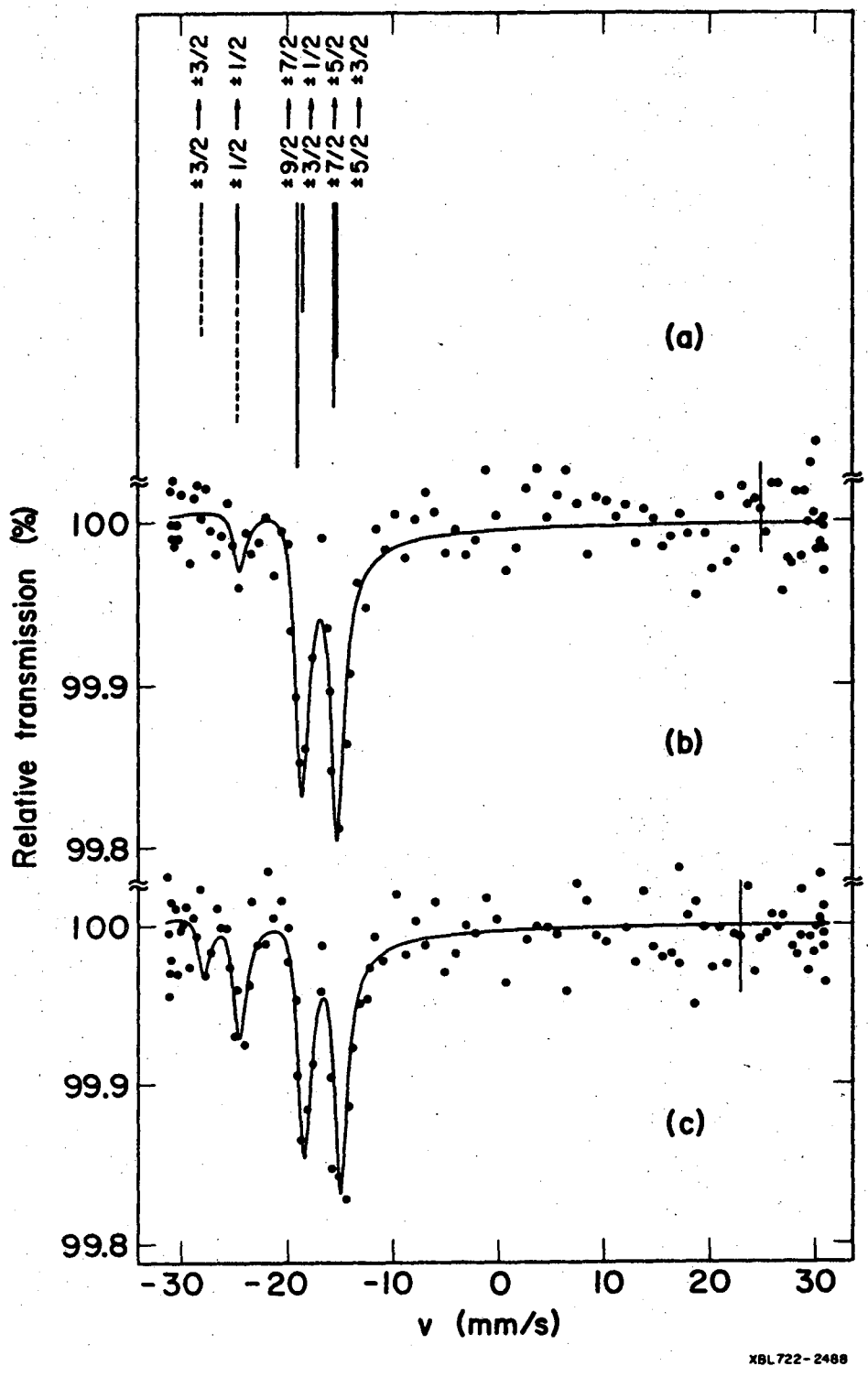

Fig. 19. $LiTaO_3$ absorber using a single line source $^{181}W(\underline{W})$. (a) The position and intensities of the individual components; solid lines are the $\Delta m \pm 1$ transition, broken lines are the $\Delta m = 0$ transition. (b) Velocity spectrum with absorber's plane perpendicular to the observation direction. (c) Velocity spectrum with absorber tilted by 45°.

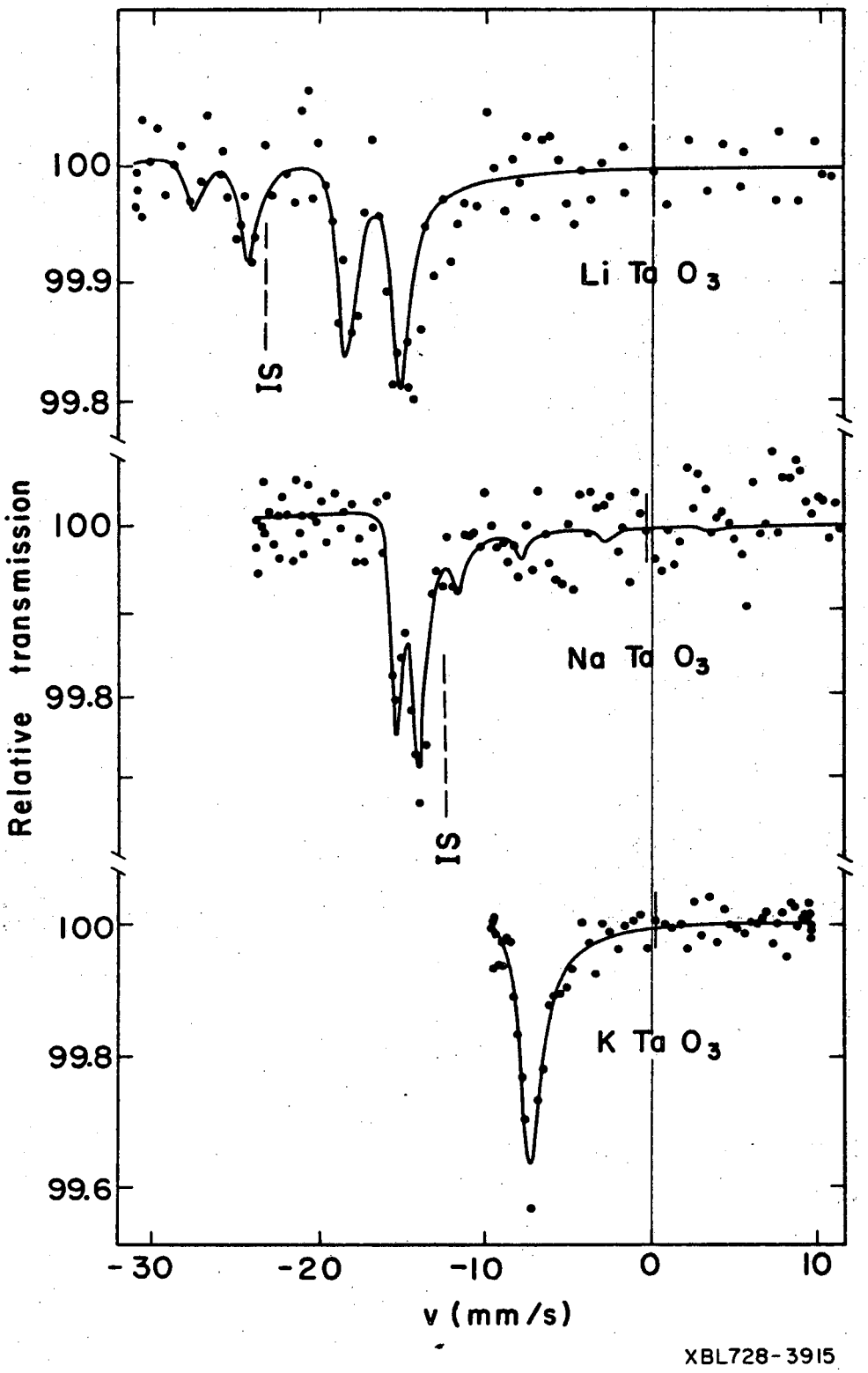

Fig. 20. Velocity spectra for the three tantalates, $LiTaO_3$, $NaTaO_3$, and $KTaO_3$. In the split spectra the isomer shift is indicated by a broken line.

Table 9. Summary of experimental results for $LiTaO_3$, $NaTaO_3$, and $KTaO_3$. Isomer shift is given relative to a Ta-metal absorber.

Compound	IS [mm/s]	$e^2qQ(7/2)$ [10^{-6} eV]	eq [10^{17} V/cm^2]	W/2 [mm/s]
$LiTaO_3$	-24.0±0.3	+2.75±0.06	+7.05±0.80	0.8±0.1
$NaTaO_3$	-13.3±0.3	-1.02±0.07	-2.61±0.45	0.4±0.1
$KTaO_3$	-8.2 ±0.2	---	---	0.8±0.1

Table 10. Comparison of EFG at the Ta/Nb sites for $LiTaO_3$ and $LiNbO_3$.

	^{7}Li quadrupole coupling constant [KH_z]	eq [V/cm^2] for Ta/Nb	
$LiTaO_3$	77.6	7.05×10^{17}	$Q(^{181}Ta) = (3.9\pm0.4)b$
$LiNbO_3$	55.2	4.55×10^{17}	$Q(^{93}Nb) = (0.2\pm0.1)b$

IX. HYPERFINE INTERACTIONS OF ^{181}Ta IN Ni

In section III, the interaction of ^{181}Ta in a W host lattice with an external magnetic field has been discussed. Due to the large parameters, only a small field of few kOe was necessary to completely split the observed levels (Fig. 4, page 13). On the other hand, due to experimental difficulties of observing a resonance for ^{181}Ta impurities in 3d hosts, hyperfine studies in ferromagnets were out of reach. The relative success of observing a resonance for ^{181}W(Ni) source above the Curie temperature (358°C) (Fig. 13, page 39), lead to the hope of a room temperature measurement [63]. The resulting velocity spectrum is shown in Fig. 21. For the room temperature measurement, the source (^{181}W diffused into a single crystal disc of Ni with the [111] direction perpendicular to the plane) was magnetized with a 1.3 kOe permanent magnet. Due to the small size of the resonance effect only the three outermost components of the transition were observed. The result was least squares fitted with constant g-factor ratio, $g(9/2)/g(7/2) = 1.78\pm0.02$ (see section III), dispersion term $2\xi(= 0.31\pm0.02)$, and an extrapolated room temperature isomer shift (see section VI).

Accounting for the external field of the permanent magnet, an internal field $H_{hf} = -89.2\pm1$ kOe was derived. Using the NMR result for $H_{hf} = -98\pm2$ kOe measured at 4.2 K by Kontani et al. [61], one gets a ratio $H_{hf}(298\ K)/H_{hf}(4.2\ K) = 0.91\pm0.02$. This value is in good agreement with a recent TDPAC study of the temperature dependence of H_{hf} for ^{181}Ta(Ni) [62] (482 keV level).

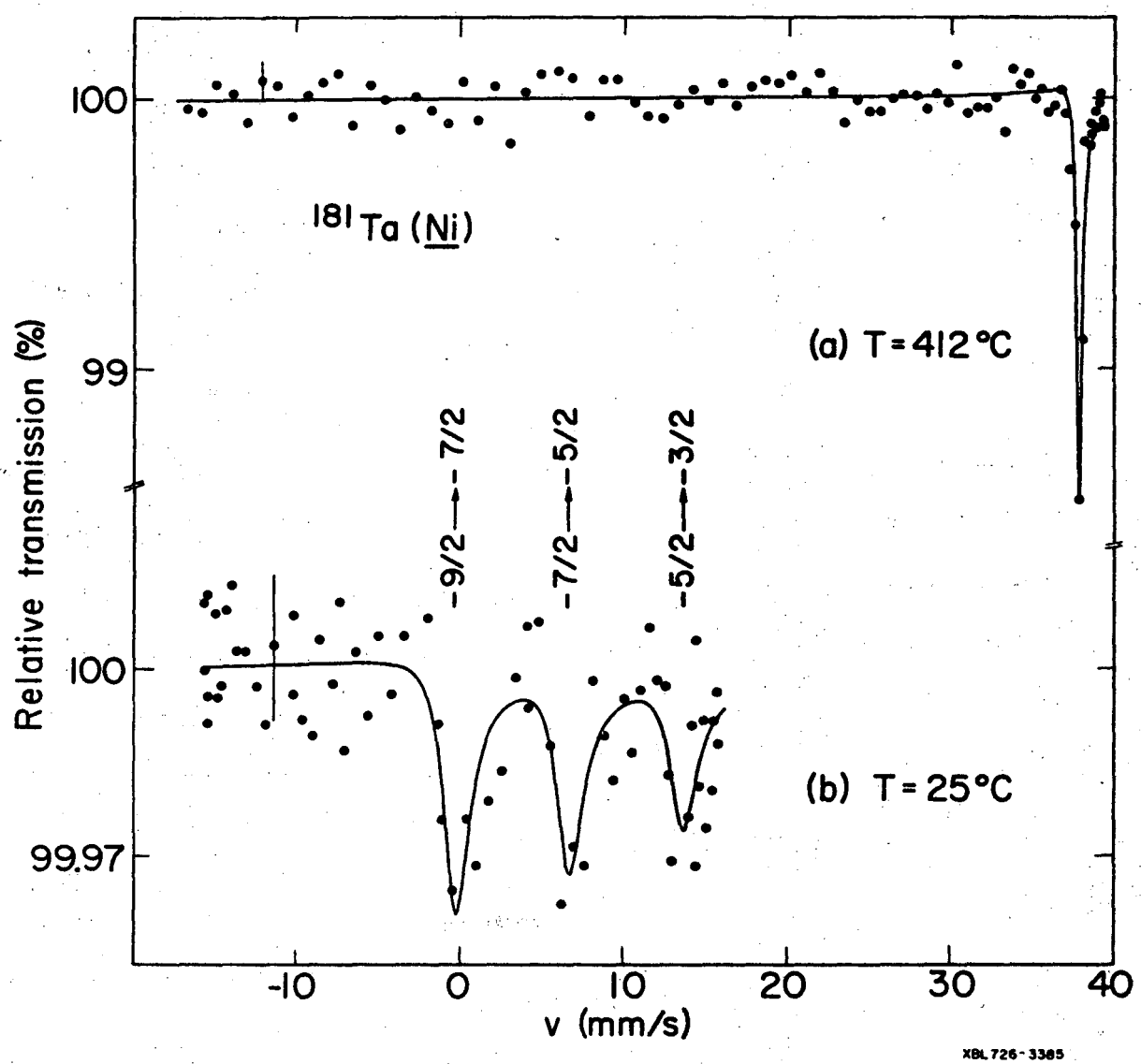

Fig. 21. Absorption spectra for ^{181}W(Ni) source (a) above the Curie point at 412°C and (b) at room temperature, using a single line Ta-metal absorber.

X. SOURCES AND ABSORBERS PREPARATIONS

A. Activity

The parent nuclide, ^{181}W, was produced by (n,γ) reaction in a reactor from 93% enriched ^{180}W metal powder. The ^{180}W enriched isotope is available from Oak Ridge National Laboratory [64] in 7% and 11% enrichments and in the chemical forms of WO_3 and W metal powder. The 93% enriched ^{180}W is available only in metal powder.

Series of sources were irradiated, first at the General Electric Vallecitos site [65] and later at the HIFR at Oak Ridge National Laboratory. Table 11 summarizes the irradiation obtained at the two sites. For each irradiation an amount of up to 4 mg, distributed in two to four capsules, was irradiated. The powder was sealed in Superseal quartz capsules of 3.5 mm diameter and about 2.5 cm long. The later sources from HIFR were very "hot", ~ 300 mc. In order to handle the activity safely, a "junior cave" [66] was used for capsule opening and subdivision of the activity. Several hot (~ 20 mc) sources were prepared from each "batch".

Table 11. Fluxes where sources were irradiated.

Site	flux (n/cm^2s)	average irradiation time	total flux range (n/cm^2)
General Electric Vallecitos	4.17×10^{14}	8 weeks	$\sim 2 \times 10^{21}$
HIFR	3×10^{15}	2-4 weeks	$4\text{-}8 \times 10^{21}$

B. Sources

The source preparations entailed preparation of host metals, deposition of activity, and then, reduction of H_2, and diffusion in high vacuum. In doing this, one wanted to keep the introduction of impurities to a bare minimum. Each process will now be discussed in turn.

Hosts The samples, all metals, were prepared from high purity and if possible single crystal materials. In the first era of sources, $^{181}W(\underline{W})$ and $^{181}W(\underline{Ta})$ were prepared from foils. These foils were heated via resistance heating, for diffusion of activity. This led to the major problem, that the foils "blew out" at a very low temperature compared with the melting point. To avoid this problem and also to facilitate the use of other pure materials, the rf heating technique was used. Discs, of about 1 mm in thickness, were cut from single crystals by a spark cutter [67]. Most single crystals were 6 mm in diameter, resulting in similar dimensions for the discs. Three equally spaced holes (a few mils in diameter) were then spark-drilled at the edges of the discs with W needles†. This then served as a means to hang the sample in the rf coil (Fig. 22).

For the hexagonal hosts, oriented discs were cut from randomly oriented single crystals. The bulk single crystals were first oriented using a laser for back reflection from an etched surface. (Planes perpendicular to the c axis tend to form upon etching--thus a bright spot is reflected from them.) Once the general direction of the c axis was known, the crystal was oriented to less than 1/2° using the Laue X-ray

---

†W needles were prepared by heating 20 mil W wire and immediately bringing it in contact with $NaNO_2$ chunks. The ensuing reaction is self-sustaining, and by skillful manning of the wire, very fine needles can be produced.

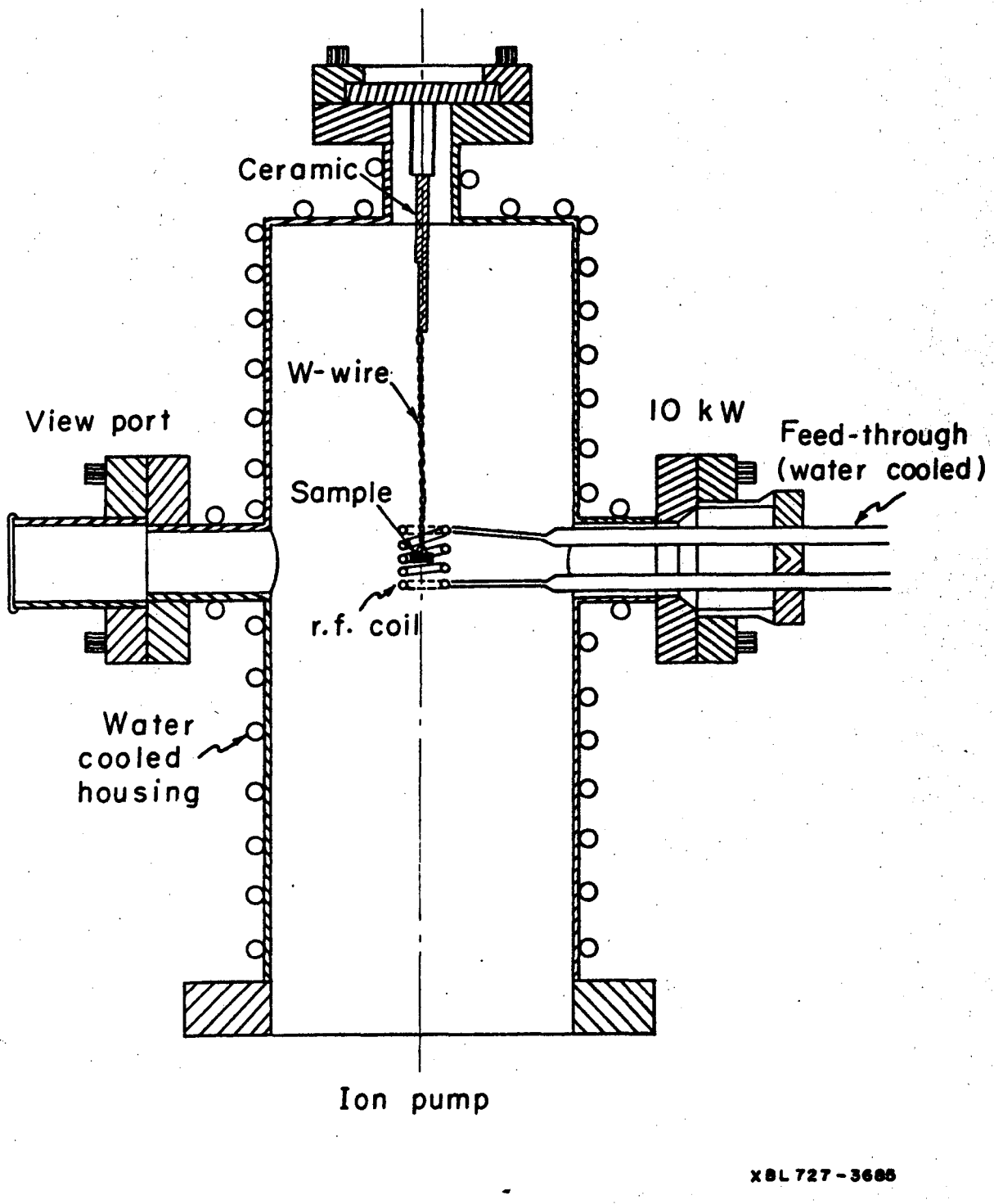

Fig. 22. High vacuum r.f. heating arrangement for source preparation.

backscattering technique, and cut with a spark-cutter, especially suited for precision cutting [68].

Once the discs were obtained, they were etched and electropolished. In addition, a crater was etched on the face. This helped to contain the activity there, as it was dropped in with H_2O--thus the drop was constrained to stay in the crater. As a final step, 3 mil W wire was strung to the holes and braided for a length of 6 cm or so. The sample was now ready to be activated.

Chemistry The activity had to be applied in a "brute" method to the samples, because W does not electroplate. The W activity in metal powder was dissolved in a small polyethylene beaker with a concentrated (1:1) solution of HNO_3/HF; usually 2 to 3 drops were sufficient. Then it was diluted with about 1/2 ml of H_2O and very slowly pumped to dryness. A few drops of H_2O were then added to the residue, and then from the resulting solution, a drop at a time was dropped onto the sample and pumped to dryness. When the desired activity was accumulated, the sample was then hung in the apparatus shown in Fig. 22. Reduction at 1/2 atmosphere of H_2 at 950°C then took place, followed by a diffusion at high vacuum of $\sim 10^{-8}$ torr. The source preparation data are summarized in Table 12.

As can be seen, the diffusion time varied from 1/2 hour up to 20 hours. One could not rely on the diffusion constants usually quoted for W in host metals, because the ^{181}W activity was not electroplated onto the hosts discs. In fact, for W in W a depth of 10,000 A° at 2,500°C is predicted in a few seconds [71]. This, however, was not the

Table 12. Preparation of sources in the transition metals.

Host metal (melting pt. °C)	Supplier & purity (%)	Diffusion Temperature (°C)	Diffusion Pressure (torr)	Diffusion Time (hrs)	Etching/polishing solution	Comments
Hf (2222)	M.R.C. 99.999/SX	1600	5×10^{-9}	8	5% perchloric/ methonol	has a transition pt. at 1740°C/outgasses
Ta (2996)	M.R.C. 99.999/SX	2500	5×10^{-8}	1	5% perchloric/ methonol	slight outgassing
W (3410)	M.R.C. 99.999/SX	2500	5×10^{-8}	30-40 minutes	NaOH 10%	
Re (3180)	M.R.C. 99.996/SX	2400	3×10^{-8}	1	5% perchloric/ methonol. (also NaOH 10%)	≠
Os (3000)	ROC/RIC 99.9/Powder	2350	2×10^{-8}	1	5% perchloric/ methonol	melted in an arc furnace from powder
Ir. (2454)	M.R.C. 99.99/SX	1850	7×10^{-9}	20	heat treatment	
Pt (1769)	M.R.C. 99.99/SX	1750	7×10^{-9}	1	heat treatment	slightly melted after diffusion
Nb (2415)	IMRD 99.99/SX	2200	6×10^{-9}	1	5% perchloric/ methonol. (after HNO_3/HF)	slight outgassing
Mo (2610)	M.R.C. 99.99/SX	2300	5×10^{-8}	1	5% perchloric/ methonol	
Ru (2500)	M.R.C. 99.99/SX	2050	4×10^{-8}	1	hot NaOH	
Rh (1966)	M.R.C. 99.99/SX	1950	1×10^{-8}	1	5% perchloric/ methonol	slightly melted during diffusion
Pd (1552)	M.R.C. 99.98/SX	1300	3×10^{-8}	10	5% perchloric/ methonol	no H_2 reduction
V (1900)	M.R.C. 99.9/PX	1750	5×10^{-8}	1	5% perchloric/ methonol	long outgassing
Ni (1453)	U.M.C. 99.995/SX	1350	3×10^{-9}	20	5% perchloric/ methonol	

S X -- single crystal

P X -- polycrystal

M.R.C. -- Material Research Corporation [69]

IMRD -- Inorganic Material Research Division, Lawrence Berkeley Laboratory

U.M.C. -- United Mineral & Chem. Corp. [78]; ROC/RIC -- Research Organic/Inorganic Chem. Corp. [74]

≠ -- resistivity ratio of $P_{300}/P_{4.2} \approx 10,500$ was measured [79]

5% perchloric/methonol was a polishing solution kept at dry-ice temperature [80]

heat treatment -- sample was heated in atmosphere to glowing, red-hot, temperature (~ 1200°C)

NaOH 10% -- was a 10% NaOH electropolishing solution at ~ 40°C

hot NaOH -- sample was boiled in fused NaOH at ~ 350°C

All samples were reduced in H_2, unless otherwise stated. Outgassing is refered to after H_2 treatment

case here. As a rule then, for metals of high melting point (2,400°C and higher), a diffusion time of about 1 hour proved to be satisfactory for diffusion temperatures of 2,000°C or higher. For the medium range (1,700 to 2,400°C), diffusing as close as possible to the melting point for a short time (about 1 hour) proved to be just as good as a long diffusion time of 10 hours or more, at somewhat lower temperatures. For low melting metals (less than 1,700°C) long diffusions were allowed. In the case of the Hf sample, one tried to keep the diffusion below the phase transition at 1740°C. It is also well known [72] that Hf, Zr, and Ti are good gas absorbers, especially for O_2, N_2, and H_2. To a lesser degree it is also true for Ta, Nb, and V [72]. This was observed in the source preparation, because these sources outgassed a long time relative to the rest, at low temperatures.

Sources of Zr were prepared, but no effect was observed. The problem for Zr and Ti hosts is that one expects a large isomer shift and quadrupole splitting, as they have hexagonal lattices. These hosts, relative to other transition metals, are not so "clean", making these cases extremely hard. On the other side of the spectrum, sources in Au and Ag were tried, including one where a gold foil was melted with W activity: it was reduced, and then melted in H_2 atmosphere, and rolled again into a very thin foil. The only effect found was the $^{181}W(\underline{W})$ line. The problem, as is indicated in Ref. 73, is that Au-W do not form an alloy up to the boiling point of gold. The same is true for Ag-W and Cu-W systems. Apparently, as was stated above, this is also the case for trace amounts of W.

C. Absorbers

The Ta metal foils were rolled to various thicknesses from 0.005", 99.996% purity Ta foil obtained from M.R.C. [69]. The general procedure was then to heat the foils resistively at ultra high vacuum ($\sim 10^{-9}$ or better). This was indeed a gamble as the thinner the foil, the lower was the temperature at which it "blew out". Thus, the following procedure was then followed:

a. $A^{1/2}$ mil foil was heated as high as possible (2300°C) before initial rolling for as long as possible (20 hours).

b. It was then rolled in a sandwich of similarly prepared foils to a thickness of about 10 mg/mm^2.

c. Step "a" was repeated (2150°C) for 20 hours.

d. Step "b" was repeated, this time to a thickness of 7 mg/cm.

e. Step "a" was repeated again, this time at 2000°C for 10-15 hours, and again repeat "b" to 3.5-4.5 mg/cm^2.

f. Final heating at ~ 1800°C.

As a heating arrangement, a 500 l/s triode pump by Aero-Vac was used, with a 10" water-cooled manifold similar in design to the source manifold in Fig. 22.

Sauer [5] made studies of Ta-metal absorbers which showed distinctly that Ta's affinity for O_2 at higher temperatures is quite destructive to the line width. Hence, the use of ultra high vacuum and high temperature for outgassing is the standard recipe. The philosophy with which one prepares a Ta absorber is that every time one manipulates the Ta foil, rolls it, anneals it, or heats it up, even at high vacuum,

one introduces new impurities. Ta is also a getter at room temperature [70]. This is especially true for H_2. In the case of H_2, however, it is reversible [70]. So it then follows that the ideal procedure would be to heat up the absorber in vacuum and then seal it rigidly in an inert gas (Ar) encasement.

Compounds Absorbers of TaC, $KTaO_3$, $NaTaO_3$, and $LiTaO_3$ were prepared as follows:

a. The powder was very finely crushed in an agate mortar.

b. It was then thoroughly shaken in an alcohol solution.

c. The solution was allowed to stand for 5 minutes.

d. The fluid was then siphoned, leaving the heavy (majority) powder behind.

e. The siphoned solution was then dried by evaporation overnight.

f. A final solution was then prepared from benzine into which ~ 15 mg of styrofoam was dissolved, and the dried compound added. After vigorously shaking this solution it was poured into a 1" diameter cylinder which had a 1/2 ml mylar bottom; and again one let the solution evaporate to dryness overnight. A thin styrofoam film then formed on the mylar sheet containing the absorber particles in a more or less uniform distribution.

The tantalates were obtained from ROC/RIC [74] and were 99.9% pure. N. H. Krikorian [75] supplied the high purity TaC.

Absorber Thickness

^{181}Ta is almost 100% abundant. It therefore follows that the ideal absorber thickness is about 0.77 mg/cm^2 [76]. All absorbers used here were 3.5 mg/cm^2 or more in thickness, clearly an order of magnitude more. Wortmann [77] has measured a spectrum with a single line source and magnetically split absorber, with no indication of improvement of the experimental line width. It follows that at this experimental state, the absorber thickness contribution to the line width is a very minor one indeed.

CONCLUSION

The 6.2 keV Mössbauer transition of ^{181}Ta has become a very powerful tool in hyperfine and subtle solid state effects. This is well demonstrated in the EFG measurements in the hexagonal transition metals and the strong dependence of the isomer shift as a function of temperature on hyperfine interaction rather than SODS. Although the best experimental line width is still an order of magnitude larger than the natural one, the highest Mössbauer resolution has already been reached, as is shown in Table 13.

Improvement of the observed resonance with respect to line width and effect would be warranted. Further applications of the resonance to studies of ferroelectric and other phase transitions, especially super conductivity, would be of high interest. Studies of alloys and tantalum chemistry are often areas to which the resonance can also be applied.

Indeed, what has been presented here is the familiarization with the ^{181}Ta resonance, which was tantalizing at times.

Table 13. Total range of observed isomer shifts R, natural line width $W_o = 2\hbar/\tau$, presently best experimental line width W and quality factors $Q_1 = R/W_o$ and $Q_2 = R/W$ for several Mössbauer transitions with good resolution for isomer shift measurements.

Isotope	gamma ray energy [keV]	IS range R [mm/s]	W_o [mm/s]	W [mm/s]	$Q_1 = \frac{R}{W_o}$	$Q_2 = \frac{R}{W}$
^{181}Ta	6.2	110	0.0064	0.069	17000	1600
^{237}Np	59.5	106	0.073	1.1	1450	96
^{243}Am	84	50	1.392	4	36	13
^{99}Ru	90	2.5	0.147	0.28	17	9
^{57}Fe	14.4	2.5	0.195	0.24	13	10
^{193}Ir	73.1	7	0.594	0.70	12	10
^{119}Sn	23.9	7	0.619	0.8	11	9

APPENDIX I

Mössbauer -- NMR

In this appendix, the effect of radiofrequency (rf) field on Mössbauer emission of nuclear Zeeman lines is discussed. The cases of ^{57}Fe 14.4 keV transition and ^{181}Ta 6.2 keV transition are examined.

Hack and Hammermesh [81] have treated the rf-field effect on the Zeeman levels assuming that nuclear resonance transitions are induced. A later approach by Gabriel [82] using Liouville operator algebra yielded similar results.

Matthias [83] tried to apply this technique experimentally to ^{57}Fe as a test for narrow Mössbauer line resonances like ^{181}Ta and ^{67}Zn. But the magnetostriction effect was overshadowing any new methodology effect for the iron case. Indications of preliminary results for ^{181}Ta are noted here.

To summarize the theoretical treatment of rf-fields on Mössbauer spectra, one can use the following derivation. First, one considers the case of no rf, i.e., two level Mössbauer decay. Then, in the notation of Wegener [84], one can write:

$$\psi_e \sim \exp(-i(E_o - i\,\Gamma/2)t) \qquad (1)$$

$$\psi_g \sim \exp(-i\,E_g\,t)$$

for the excited and ground levels. The emission amplitude E(t) is proportional to $\psi_g^* \cdot \psi_e \sim \exp(-i(\omega_o - i\,\Gamma/2)t)$ where $\omega_o = E_e - E_g$, is the γ-ray energy for the transition between the excited and ground state,

$\Gamma = 1/\tau$ where τ is the mean life of the excited state. Thus, taking the Fourier transform of E(t) one gets

$$F(\omega') = \int_0^\infty E(t)\ \exp(i\omega' t)dt \sim \frac{1}{(\omega' - \omega_o) + i\ \Gamma/2} \tag{2}$$

from this one gets the intensity of the emission

$$I(\omega') = |F(\omega')|^2 \sim \frac{1}{(\omega' - \omega_o)^2 + (\Gamma/2)^2} \tag{3}$$

which is the general form for the Mössbauer emission spectra.

Now, if the excited and ground levels were split in a magnetic field, then the transition from an excited sublevel to a ground sublevel could be treated in the same manner as above:

$$\begin{aligned} \psi_{m_e} &\sim \exp(-i(E_{m_e} - i\ \Gamma/2)t) \\ \psi_{m_g} &\sim \exp - i\ E_{m_g}\ t \end{aligned} \tag{4}$$

Summing over all sublevels m_e and m_g and following steps (2) and (3) above, one then gets

$$I(\omega') \sim \sum_{\substack{m_e \\ m_g}} L(m_e, m_g, \theta)\ \frac{1}{(\omega' - \omega_o - \omega_e m_e + \omega_g m_g)^2 + \Gamma^2/4} \tag{5}$$

where $L(m_e, m_g, \theta)$ accounts for the individual intensities and allowed transitions and θ is the angle between H_o, the magnetic field, and

direction of observation ($\theta = < (\underset{\sim}{H}_o, \underset{\sim}{k})$), ω_e and ω_g correspond to the excited and ground state sublevel splittings.

If one now applies an rf-field, H_1 perpendicular to H_o, one gets a resulting field, H_R, which is the effective magnetic field in the rotating frame [85]. Thus, one now has a new quantization axis z' in the rotating frame. Along the z' then

$$\psi_{M_e} = e^{-iE_{M_e}t} e^{-(\Gamma/2)t}$$
$$\psi_{M_g} = e^{-iE_{M_g}t} \tag{6}$$

One now has to transform this to the laboratory frame via the rotation operator $D^I(0,\beta,0)_{m'm}$:

$$\psi_{m_e} = \sum_{M_e} d^{I_e}_{m_e M_e}(\beta_e)\, e^{-i\omega M_e t}\, \psi_{M_e}$$
$$\psi_{m_g} = \sum_{M_g} d^{I_g}_{m_g M_g}(\beta_g)\, e^{-i\omega M_g t}\, \psi_{M_g} \tag{7}$$

Summing over all m_e and m_g, and again, following steps 2 and 3 above, one gets

$$I(\omega',\omega) \sim \sum_{\substack{m_e \\ m_g}} L(m_e, m_g, \theta) \sum_{\substack{M_e \\ M_g}} \frac{|d^{I_e}_{m_e M_e}(\beta_e)|^2\, |d^{I_g}_{m_g M_g}(\beta_g)|^2}{(\omega' - \omega_o + \omega(M_e - M_g) - a_e M_e + a_g M_g)^2 + \Gamma^2/4} \tag{8}$$

where $a_{\substack{e\\g}} = \omega_{\substack{e\\g}}\sqrt{(1 + \omega/\omega_{\substack{e\\g}})^2 + (\omega_1/\omega_{\substack{e\\g}})^2}$ is the effective splitting of the sublevels along z', ω is the angular frequency of H_1 ($\sim \omega_1 \cos(\omega t)$), and

$$\cos(\beta_{\substack{e\\g}}) = \frac{\omega_{\substack{e\\g}} - \omega}{a_{\substack{e\\g}}} \quad ; \quad \sin(\beta_{\substack{e\\g}}) = \frac{\omega_1}{a_{\substack{e\\g}}}$$

I_e and I_g are the spins for the excited and ground states, respectively.

Equation (8), then, is the expression for the Zeeman split Mössbauer emission spectrum with rf.

The case of ^{57}Fe, 14.4 keV transition can now be examined in equation (8). For ^{57}Fe, $I_e = 3/2$, $I_g = 1/2$, and in iron lattice† the hyperfine field is $H_o = 330$ kOe. $\mu_e = 0.15\ \mu_N$ and $\mu_g = 0.09\ \mu_N$ [86]. Thus, one has two resonant frequencies corresponding to the excited and ground state sublevels, which are 26 and 45.4 MH_z. Equation (8) is plotted for ^{57}Fe in Fig. I-1. There one has the velocity spectra for several frequencies off and on resonance. The broken line spectra are the no-rf case.

---

†One of the requirements for NMR transition, is that $\omega_1\tau \sim 1$; that is the rf field amplitude must be large enough to induce a transition during the lifetime, τ, of the nucleus. For ^{57}Fe $\tau \sim 10^{-7}$s, thus one needs rf fields $H_1 = \frac{\omega_1}{\gamma}$ of the order of 10^4 Oe. This can be achieved only in a ferromagnetic material where one has the enhancement factor [87]. On the other hand, for ^{181}Ta due to the longer half life (6.8 μs) and the large nuclear moments, only a few gauss are needed for H_1 if $H_o = 2$ kOe.

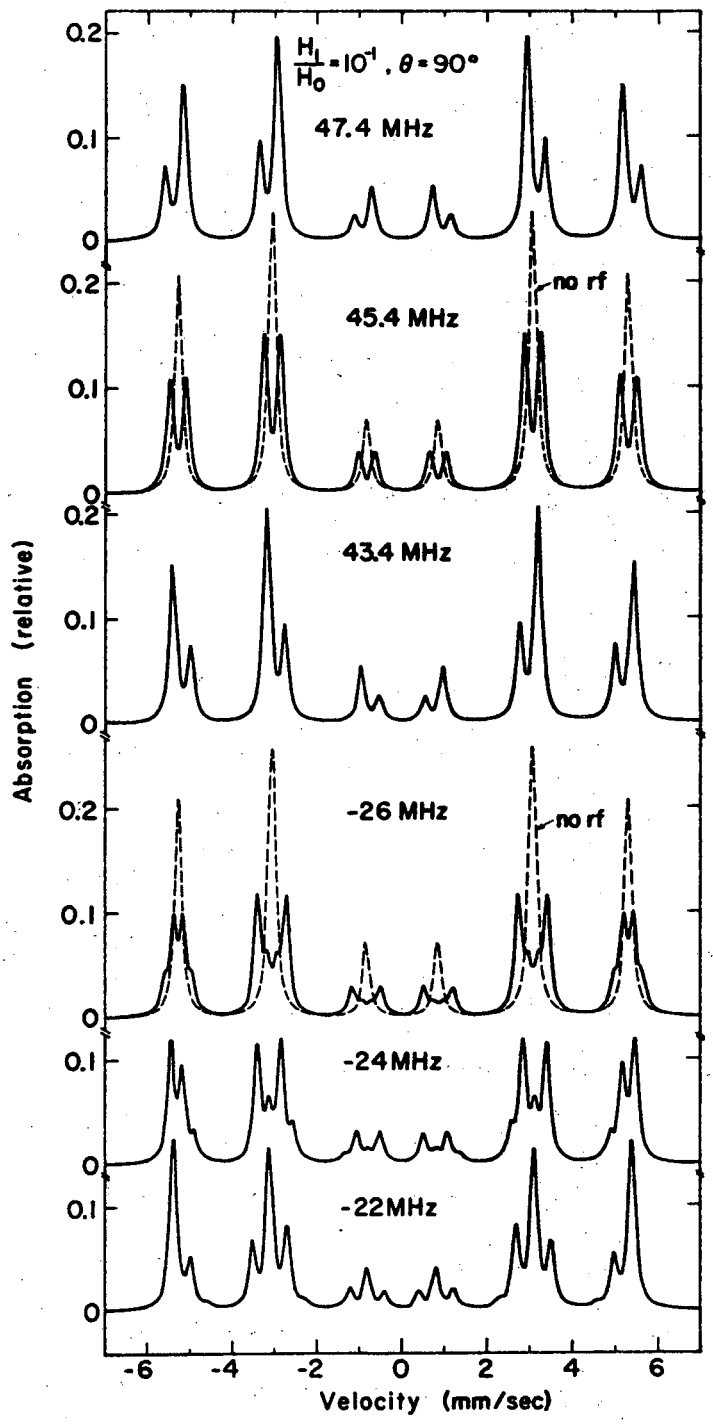

Fig. I-1. Velocity spectra of ^{57}Fe after equation (8) for a source with magnetic splitting (H_o = 330 kOe) for various frequencies. ($\underline{H}_o \perp \underline{k}$, Γ = 1.1 MHz.)

In Fig. I-2, equation (8) is plotted for fixed velocity ($v = 0$) as a function of frequency, analyzed by a split absorber. To visualize this, the "area" of the broken line curve in Fig. I-1 "multiplied" by the overlapping "area" of the solid curve, is plotted as a function of frequency (Fig. I-2). In reality, one measures the transmitted spectra, that is the inversion of the spectra shown in Figs. I-1,2.

An experiment was conducted for ^{57}Fe with similar set up to the curves of Fig. I-2. The results are shown in Fig. I-3. The effect at the expected resonance positions was of opposite sign. This is due to the magnetostriction effect (see Appendix II). Thus, ^{57}Fe proved to be a poor case for the NMR effect.

In Fig. I-4, equation (8) is plotted for the case of ^{181}Ta. The experimental arrangement in consideration is similar to the one of ^{57}Fe in Fig. I-2, and is the same as the one discussed in section III (page 17).

The experimental results for ^{181}Ta are reproduced here in Fig. I-5, and they are in agreement with the theory of Fig. I-4. One should note that the theory in Fig. I-4 is for a natural line width of the ^{181}Ta 6.2 keV γ-rays, and that the experimental one is about 15 times that. Curves similar to the ones in Fig. I-4 (not shown here) for a larger line width, mostly reduce the size of the effect and somewhat broaden the "lines"; the overall envelope or shape is the same.

In conclusion, the 6.2 keV transition of ^{181}Ta proves to be a better testing ground for the methodology of Mössbauer NMR. Clearly, a narrower line width in this case is required. However, as shown earlier, ^{181}Ta is very vulnerable to impurities and lattice defects. Thus, it is hard to conceive that the method would be applicable to other extreme narrow resonance lines.

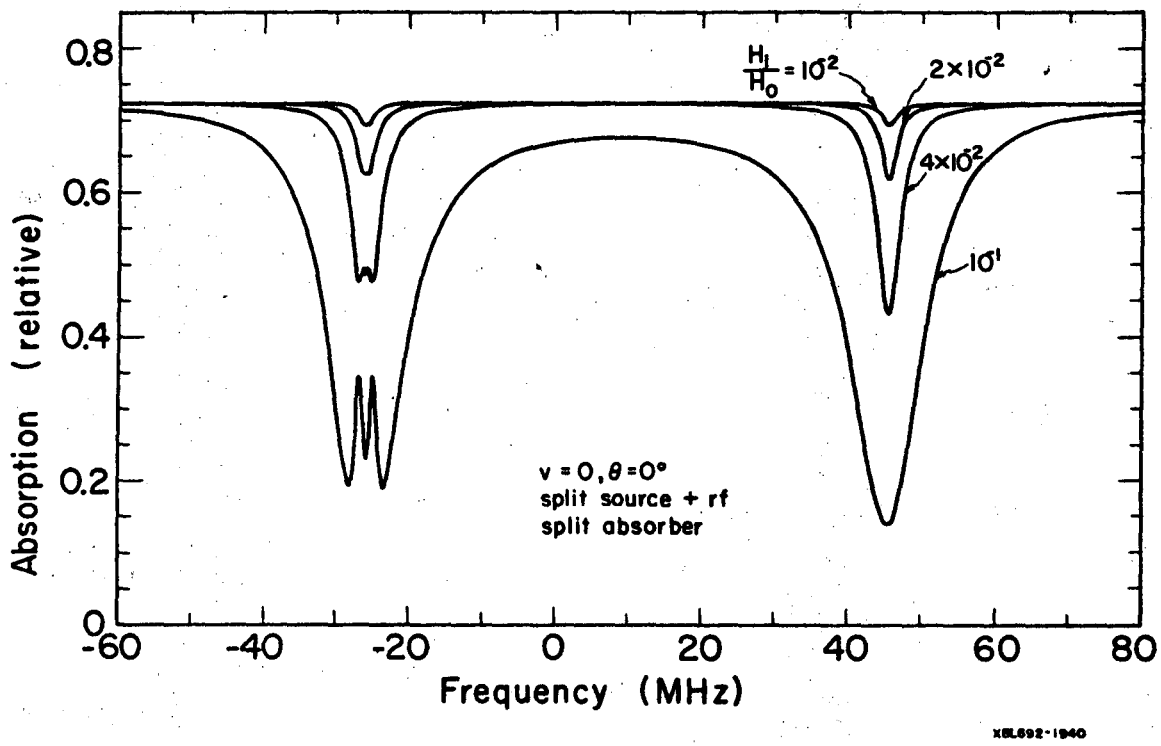

Fig. I-2. Frequency spectra at zero velocity of ^{57}Fe after equation (8), for various ratios of H_1/H_o, with source condition as in Fig. I-1, and analyzed with a split absorber (broken line spectra in Fig. I-1).

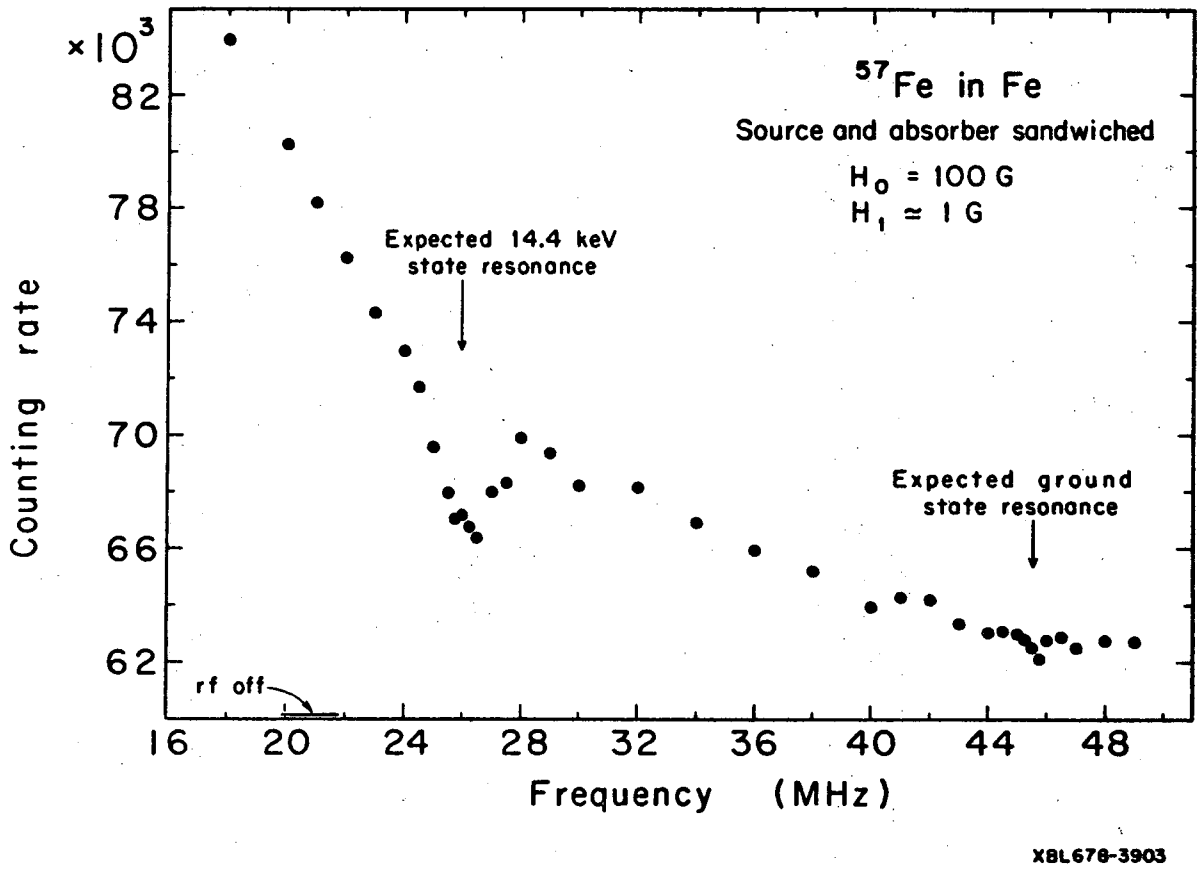

Fig. I-3. Experimental result in an attempt at NMR in ^{57}Fe. The result here is completely accounted for by magnetostriction. The resonance effects have opposite sign to the expected sign for Fig. I-2. Also, the sloping background is of magnetostriction origin, especially the ratio to rf off.

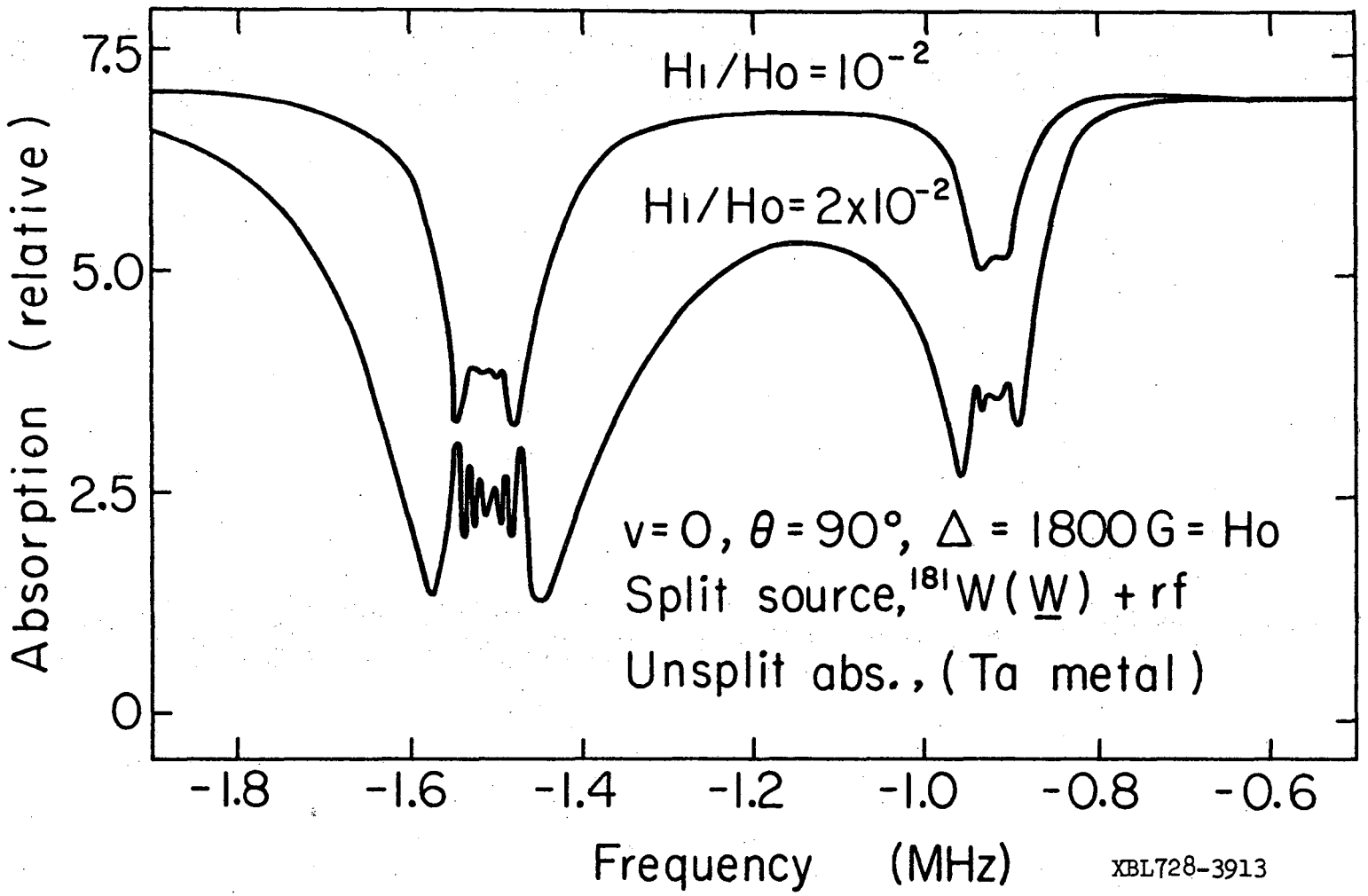

Fig. I-4. Theoretical frequency spectra after equation (8), for special case of ^{181}Ta 6.2 keV with source and absorber as noted. N.B. for transmission spectra the effect above is inverted.

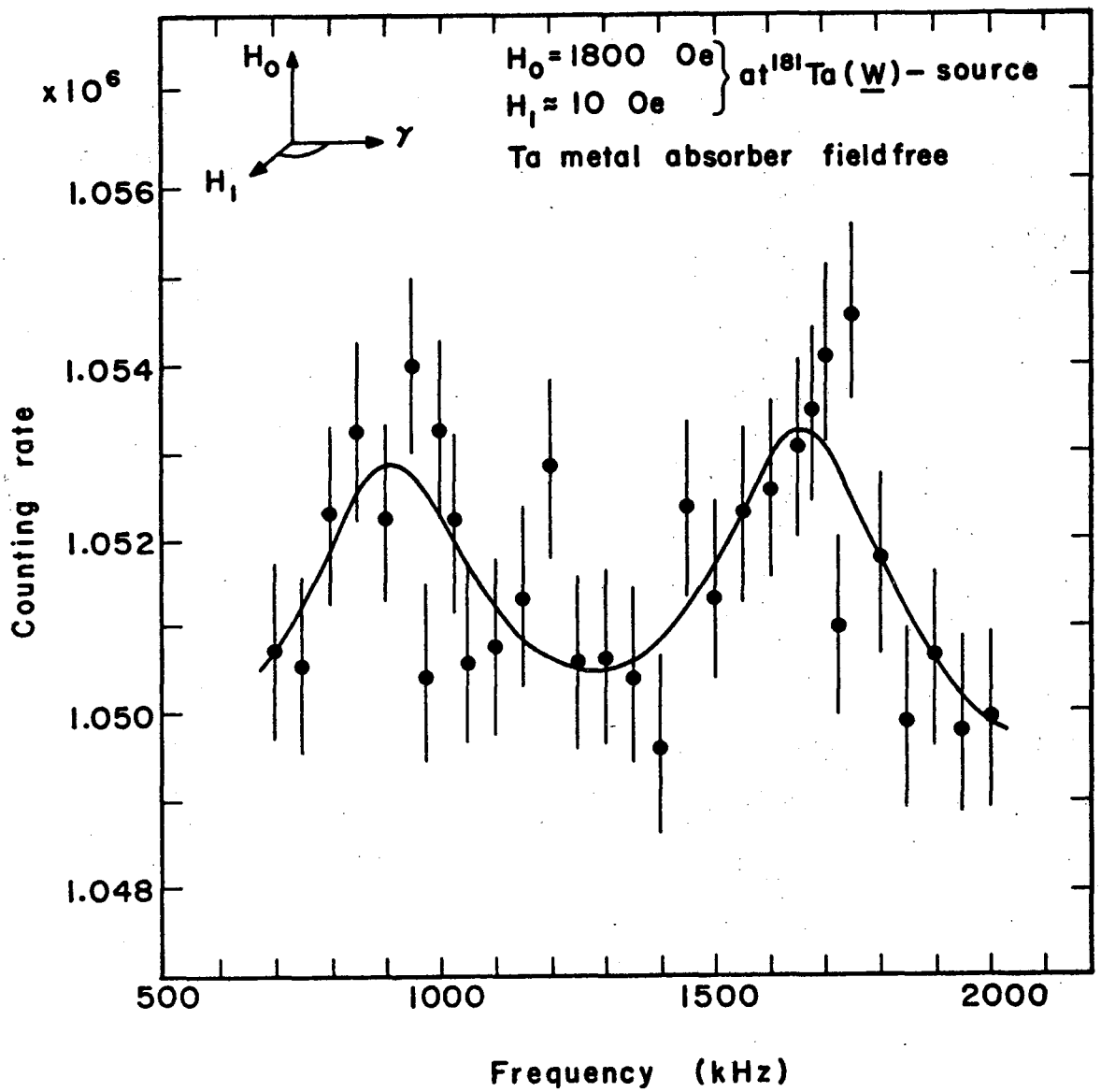

XBL713-3188

Fig. I-5. Experimental transmission spectra for ^{181}Ta for the same arrangement as the theoretical one in Fig. I-4. (rf off count rate is 1.051×10^6.)

APPENDIX II

Magnetostriction, via rf, Effect on $^{57}Fe(Fe)$ Mössbauer Spectra

When a ferromagnetic material is magnetized its physical dimensions are changed by a few parts per million, such changes are referred to as magnetostriction [88]. Now, when radiofrequency is applied to ^{57}Fe nuclei in a ferromagnetic material, large rf fields are produced. The ensuing result is a frequency modulation of the nuclei. This is very vivdly shown in the production of sidebands for the Mössbauer resonance lines (Fig. II-2). In essence, the nucleus which emits a γ-ray ($\omega \sim 10^{19}$) is "physically" modulated at frequency $\Omega \sim 10^{7}$. Classically then, one has sidebands around the radiating frequency ω at intervals $\pm n\Omega$, $n = 1,2,3, \ldots$, and the intensity of the nth sideband is given by the Bessel function $J_n^2(m)$, where m is the modulation index. Similar results were obtained by Perlow [89] and Heiman, Pfeifer, and Walker [90]. The modulation index is discussed in these references, and is given by $m = \Omega A/c$ where A is proportional to the magnetostrictive constant, the material dimensions, and the magnetizations involved.

Sidebands for Mössbauer resonance lines were also obtained by Ruby and Bolef [91], who physically modulated the source with a piezoelectric quartz crystal.

In light of Fig. II-1, one can then reconstruct the "destruction" of the Mössbauer resonance at zero velocity for the arrangement used in Fig. I-3. The recurrence of resonance at 26 MHz (and 45.4 MHz) is just an overlapping of sidebands and resonance lines.

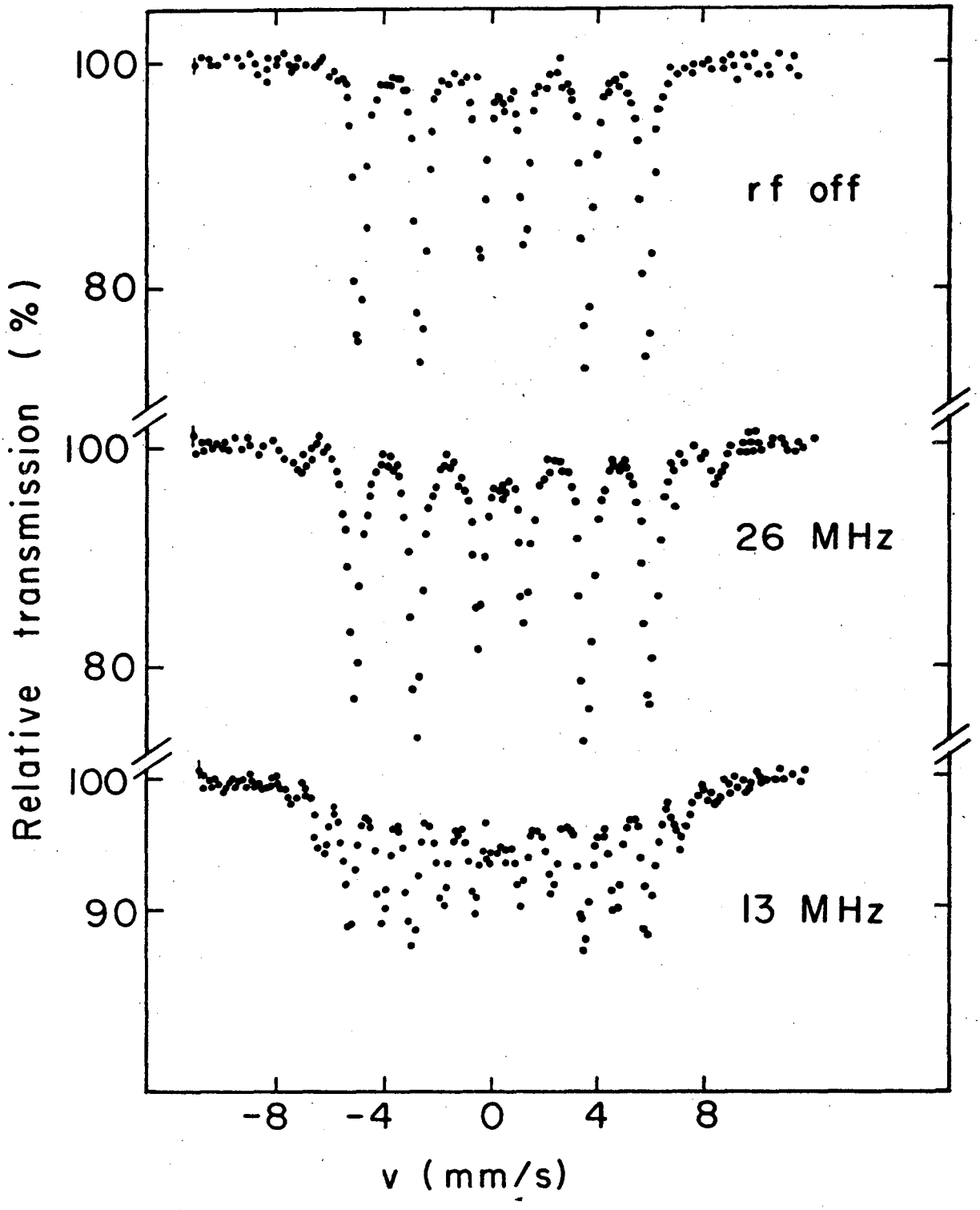

XBL729-3960

Fig. II-1. rf effects on Mössbauer spectrum of ^{57}Fe. A single-line source and a split absorber (in rf) was used.

APPENDIX III

Systematics of Isomer Shifts of ^{57}Fe, ^{197}Au, and ^{99}Ru Impurities in Transition Metals

The ^{57}Fe results are reproduced in Fig. III-1. All values there are according to Quam [44], except the ones for Ru and Os hosts. These values were measured in conjunction with the Ta work, with the results of a single-line spectra with isomer shifts of -0.134±0.002 and -0.144±0.002 mm/s for the Ru and Os hosts, respectively.

The contributed paper† "Systematics of Isomer Shifts for Impurities of ^{197}Au and ^{99}Ru in Transition Metals" is also presented in this appendix.

---

†Presented under co-authorship with G. Kaindl, at the International Conference on the Applications of the Mössbauer Effect, held in Israel on August 1972.

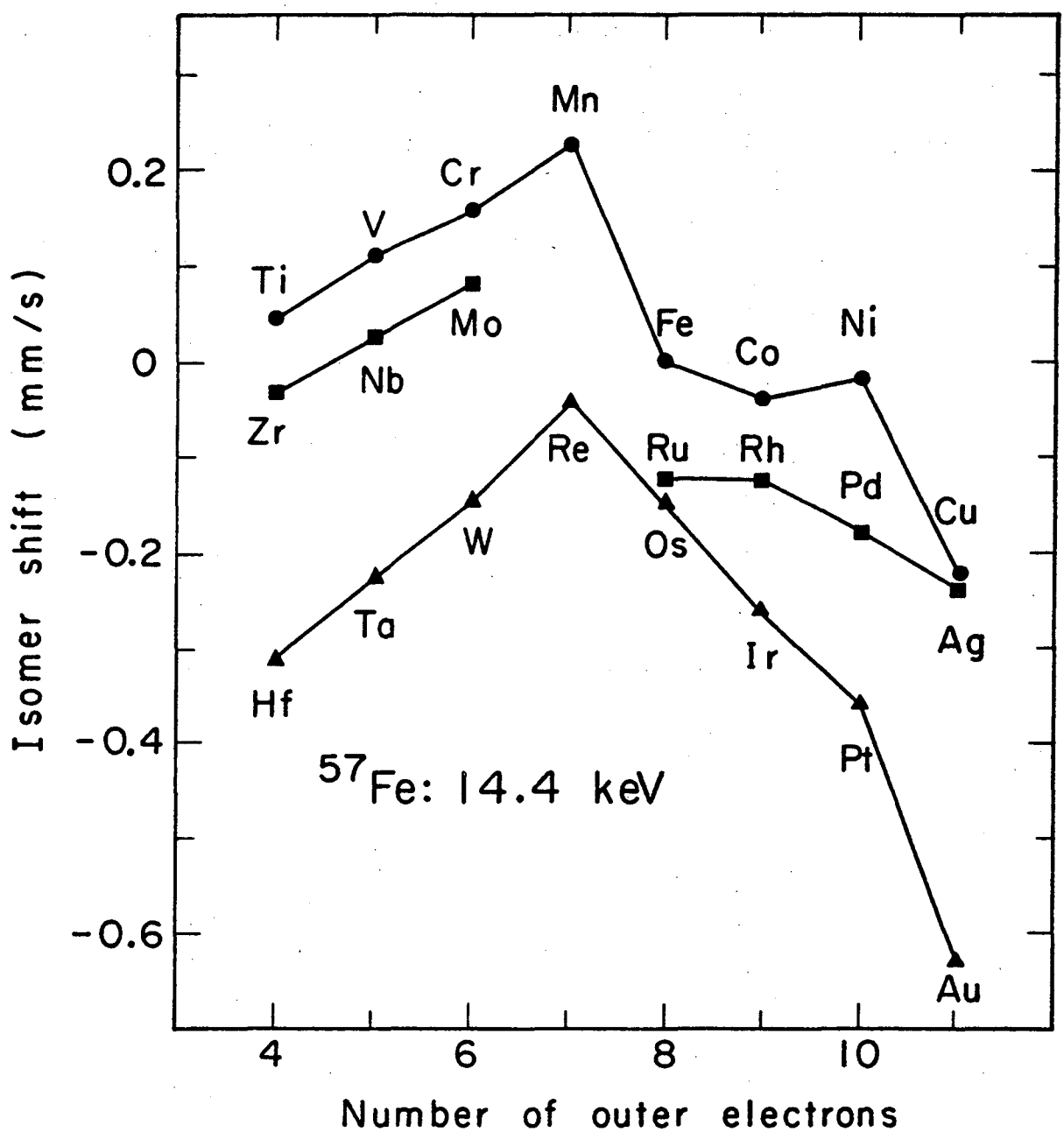

XBL729-3961

Fig. III-1. Systematics of the isomer shifts for ^{57}Fe impurities in the transition metals.

0 0 0 0 3 8 0 7 0 9 2

Systematics of Isomer Shifts for Impurities of ^{197}Au and ^{99}Ru in Transition Metals

G. Kaindl and D. Salomon

Lawrence Berkeley Laboratory
University of California
Berkeley, California 94720

Recently, large isomer shifts (IS) of the 6.2 keV γ rays of ^{181}Ta in transition metal hosts have been observed,[1,2] which vary systematically with the number of outer electrons of the host elements[2,3] in a similar way as those of the 14.4 keV γ rays of ^{57}Fe.[4] We now report a similar study for impurities of ^{197}Au and ^{99}Ru, using the well-known 77 keV and 90 keV Mössbauer transitions.

All the experiments reported here were performed with sources of ^{197}Pt and ^{99}Rh(Ru), respectively, melted into the different host metals using an argon arc-furnace. With this technique, the impurity concentration could be kept less than 0.2 at .% for the ^{197}Au experiments, and less than 0.5 at .% for the ^{99}Ru case. The measurements were done at 4.2 K, using single-line absorbers of Au metal (50 mg/cm^2) and ^{99}Ru metal (26 mg/cm^2), respectively. The total ranges of the observed ISs exceed the experimental linewidths by factors of 4 (for Au) and 3 (for Ru).

The IS results are plotted in Fig. 1 against the number of outer electrons in the same way as previously done for ^{57}Fe [4] and ^{181}Ta.[2,3] Since the changes of the mean square nuclear charge radii are known and positive for both Mössbauer transitions,[5,6] the total electron density at the nucleus $(e|\psi(0)|^2$ increases in both cases with increasing IS. With the exception of ^{197}Au(Zr) and ^{197}Au(Ti), $e|\psi(0)|^2$ increases when proceeding from a 5d to a 4d and further to a 3d element in a vertical column of the periodic system. The same general behaviour has been observed for ^{57}Fe and ^{181}Ta. It may be explained by a pseudo-potential approach,[7] taking into account orthogonalization effects introduced by the extra atomic states associated with the impurity atom. The systematic variations of the isomer shifts in a horizontal row reflect mainly changes in the band structure of the host metals.

References:

1. D. Salomon, G. Kaindl, and D. A. Shirley, Phys. Letters 36A, 457 (1971).
2. G. Kaindl and D. Salomon, this conference.
3. G. Kaindl, D. Salomon, and G. Wortmann, to be published.
4. S. M. Quaim, Proc. Phys. Soc. 90, 1065 (1967).
5. W. Potzel, F. E. Wagner, R. L. Mössbauer, G. Kaindl, and H. E. Seltzer, Z. Phys. 241, 179 (1971).

6. G. K. Shenoy and G. M. Kalvius, in Hyperfine Interactions in Excited Nuclei, edited by G. Goldring and R. Kalish (Gordon and Breach (1971) p. 1201.
7. X. A. da Silva, A. A. Gomes, and J. Danon, Phys. Rev. 4B, 1161 (1971).

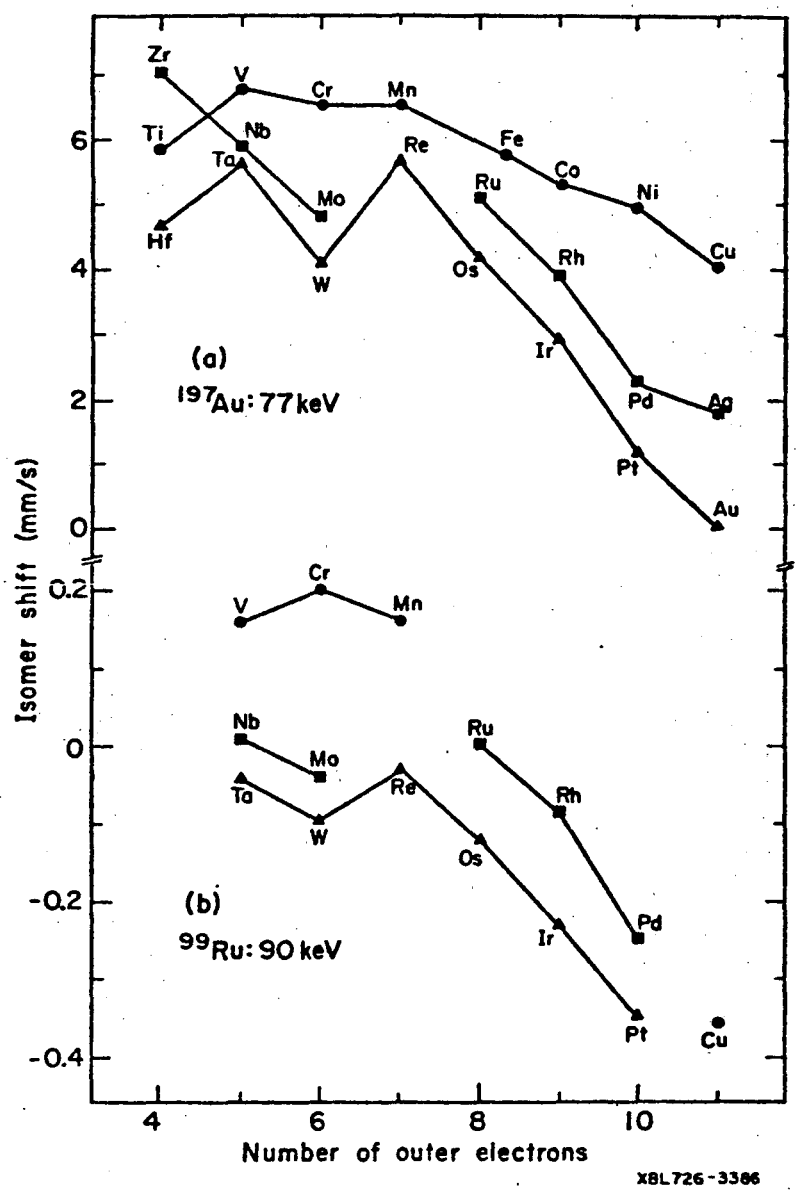

Fig. 1. Isomer shifts of the 77 keV γ rays of ^{197}Au (a) and the 90 keV γ rays of ^{99}Ru (b) plotted against the number of outer electrons of the 3d, 4d, and 5d transition metal hosts. The isomer shifts for ^{197}Au are given with respect to a Au metal absorber, and those for ^{99}Ru with respect to a Ru metal absorber.

REFERENCES

1. A. H. Muir and F. Boehm, Bull. Am. Phys. Soc. 4, 367 (1959).

2. S. G. Cohen, A. M. Arinov, and J. I. Budnick, Phys. Letters 12, 38 (1964).

3. W. A. Steyeret, R. D. Taylor, E. K. Storms, Phys. Rev. Letters 14, 739 (1965).

4. C. Sauer, E. Matthias, and R. L. Mössbauer, Phys. Rev. Letters 21, 961 (1968).

5. C. Sauer, Z. Physik 222, 439 (1969).

6. H. Frauenfelder, The Mössbauer Effect (Benjamin, New York, 1962).

7. G. K. Wertheim, Mössbauer Effect: Principles and Applications (Academic Press, New York, 1964).

8. R. L. Mössbauer and M. J. Clauser, "Recoilless Absorption of Rays", in Hyperfine Interactions, A. J. Freeman and R. B. Frankel, editors (Academic Press, New York, 1967).

9. A. Abragam, L'Effect Mössbauer (Gordon and Breach, New York, 1964).

10. A. H. Muir, Jr., Nucl. Phys. 68, 305 (1965).

11. D. A. Shirley, Rev. Mod. Phys. 36, 339 (1964).

12. e.g., R. M. Lieder, N. Buttler, K. Killig, and K. Beck, Z. Physik 237, 137 (1970).

13. P. Steiner, E. Gerdau, W. Hautsch, and C. Steenken, Z. Physik 221, 281 (1960).

14. C. M. Lederer, J. M. Hollander, and I. Perlman, Table of Isotopes (John Wiley and Sons, New York, 1967) Sixth Edition.

15. G. Kaindl, M. R. Maier, H. Schaller, and F. Wagner, Nucl. Inst. 66, 277 (1968).

16. L. W. Fagg and S. S. Hanna, Rev. Mod. Phys. 31, 711 (1959).

17. G. Kaindl and D. Salomon, Phys. Letters 32B, 364 (1970), and D. Salomon and G. Kaindl, Lawrence Berkeley Laboratory, Nuclear Chemistry Annual Report, UCRL-20426 (1970) page 215.

18. G. T. Trammel and J. P. Hannon, Phys. Rev. 180, 337 (1969).

19. Yu M. Kagan, A. M. Afanasev, and V. K. Voltovetskii, JETP Letters 9, 91 (1969).

20. G. Kaindl and D. Salomon, Bull. Am. Phys. Soc. 16, 640 (1971).

21. L. H. Bennett and J. I. Budnick, Phys. Rev. 120, 1812 (1960).

22. U. Hauser, Nucl. Phys. 24, 553 (1965).

23. H. K. Walter, A. Weitsch, and P. Kienle, Z. Physik 175, 520 (1963).

24. S. Koicki, A. Koicki, and G. T. Wood, Nucl. Phys. 49, 161 (1963).

25. O. Prior, F. Boehm, and S. G. Nilsson, Nucl. Phys. A110, 257 (1968).

26. Table of mass absorption coefficients Norelco-Reporter, M/J (1962).

27. A. Abragam and F. Boutron, C. R. Aca. Sci. 252, 2404 (1961).

28. G. Kaindl, D. Salomon, and G. Wortmann, Phys. Rev. Letters 28, 952 (1972), and D. Salomon, G. Kaindl, and G. Wortmann, Bull. Am. Phys. Soc. 17, 86 (1972).

29. L. Lindgren, Ark. Fys. 29, 553 (1965).

30. e.g., E. Segrè, Nuclei and Particles (Benjamin, New York, 1965).

31. G. Kaindl and D. Salomon, Phys. Letters 40A, 179 (1972).

32. G. Kaindl and D. Salomon, Bull. Am. Phys. Soc. 17, 681 (1972).

33. F. D. Feiock and W. R. Johnson, Phys. Rev. 187, 39 (1969).

34. R. Sternheimer, private communication (1972).

35. R. E. Watson, A. C. Gossard, and Y. Yafet, Phys. Rev. 140, A375 (1965).

36. F. W. DeWette, Phys. Rev. 123, 103 (1961).

37. R. M. Lieder, N. Butler, K. Killig, K. Beck, and E. Bodenstedt, in Hyperfine Interactions in Excited Nuclei, G. Goldring and R. Kalish, editors (Gordon and Breach, New York, 1971) page 449.

38. G. Kaindl, H. Rinneberg, and D. Salomon, to be published.

39. J. Buttet and P. K. Baily, Phys. Rev. Letters 24, 1220 (1970).

40. P. E. Gregers-Hansen, M. Krusius, and G. R. Pickett, Phys. Rev. Letters 27, 38 (1971), and references there-in.

41. F. E. Wagner, Technical University Munich, private communication (1971).

42. P. Boolchand, B. L. Robinson, and S. Jha, Phys. Rev. 187, 475 (1969).

43. G. Wortmann, Phys. Letters 35A, 391 (1971).

44. S. M. Quaim, Proc. Phys. Soc. (London) 90, 1065 (1967).

45. G. Kaindl and D. Salomon, contributed paper to the International Conference on Applications of the Mössbauer Effect, Israel (1972).

46. G. K. Shenoy and G. M. Kalvius, in (see Ref. 37) page 1201.

47. R. L. Mössbauer, M. Lengsfeld, W. von Lieres, W. Potzel, P. Teschner, F. E. Wagner, and G. Kaindl, Z. Natuforschung 26a, 344 (1971); F. E. Wagner, private communication.

48. M. Faltens and D. A. Shirley, J. Chem. Phys. 53, 4249 (1970).

49. R. V. Pound and G. A. Rebka, Jr., Phys. Rev. Letters 4, 274 (1960).

50. B. D. Josephson, Phys. Rev. Letters 7, 341 (1960).

51. R. V. Pound, G. B. Benedek, and R. Drever, Phys. Rev. Letters 7, 405 (1961).

52. G. M. Rothberg, S. Guimard, and N. Benczer-Koller, Phys. Rev. 1B, 136 (1970).

53. R. D. Taylor and E. K. Storms, Bull. Am. Phys. Soc. 14, 836 (1969).

54. R. Ingalls, H. G. Drickhamer, and G. de Pasquali, Phys. Rev. 155, 165 (1967).

55. L. D. Roberts, D. O. Patterson, J. O. Thomson, and R. P. Levey, Phys. Rev. 179, 656 (1969).

56. Extrapolated from "Relativistic Dirac-Fock Calculations for Os Ions" by J. B. Mann, Los Alamos (1971).

57. T. Muto, S. Kobayasi, M. Watanabe, and H. Kozima, J. Phys. Chem. Solids 23, 1303 (1962).

58. L. E. Toth, Transition Metal Carbides and Nitrides (Academic Press, New York, 1971).

E. Dempsey, Phil. Mag. 8, 285 (1963); R. G. Lye and E. M. Logothetis, Phys. Rev. 147, 622 (1966); V. Ern and A. C. Switendick, Phys. Rev. 137, A1927 (1965).

59. G. Kaindl, D. Kucheida, W. Potzel, F. E. Wagner, Ursel Zahn, and R. L. Mössbauer, in same reference as 37, page 595.

60. G. E. Peterson and P. M. Bridenbaugh, J. Chem. Phys. 48, 3402 (1968).

61. M. Kontani and J. Itoch, J. Phys. Soc. (Japan) 22, 345 (1967).

62. J. S. Barrett, J. A. Cameror, and Z. Zamori, Can. J. Phys. 50, 619 (1972).

63. G. Kaindl and D. Salomon, in same conference as in Ref. 45.

64. Oak Ridge National Laboratory, Isotope Division, Oak Ridge, Tennessee.

65. General Electric Co., Vallecitos Atomic Laboratory, Pleasanton, Calif.

66. Safety Services, Lawrence Berkeley Laboratory, Berkeley, Calif.

67. Materials Research Ltd., Cambridge, England.

68. Inorganic Materials Research Division, Lawrence Berkeley Laboratory, Berkeley, Calif.

69. Materials Research Corp., Orangeburg, New York.

70. Gmelins, Handbuch der Anorganischen Chemie Ta (Vol. 50) 1969.

71. R. L. Andelin, Los Alamos Sci. Lab. Report LA-2880 (1963).

72. Gmelins, same reference as 70, Hf (Vol. 43), Zr (Vol. 42), Ti (Vol 41).

73. R. P. Elliott, Constitution of Binary Alloys, First Supplement (McGraw-Hill, New York, 1965).

74. Research Organic/Inorganic Chemical Corp., Sun Valley, Calif.

75. The author is indebted to Dr. N. H. Krikorian, Los Alamos Sci. Lab. for the high purity TaC.

76. U. Shimony, Nucl. Instr. Methods 37, 348 (1965).

77. G. Wortmann, Thesis, Technical University, Munich (1971).

78. United Mineral and Chemical Corp., New York, New York.

79. B. B. Triplett, University of California, Berkeley, private communication (1971).

80. E. H. Hopkins, D. T. Peterson, and N. Baker, Iowa State University Report IS-1184 (1966).

81. M. N. Hack and M. Hammermash, Nuovo Cimento 19, 546 (1961).

82. H. Gabriel, Phys. Rev. 184, 359 (1969).

83. E. Matthias, in Hyperfine Structure and Nuclear Radiations, E. Matthias and D. A. Shirley, editors (North-Holland Publishing Co., 1968) page 815.

84. H. Wegener, Der Mössbauer Effekt, (Bibliographisches Institut, Mannheim, 1965) page 11.

85. I. I. Rabi, N. F. Ramsey, and J. Schwinger, Rev. Mod. Phys. 26, 167 (1954).

86. V. Shirley, Table of Nuclear Moments in same reference as 37, page 1255.

87. A. M. Portis and R. H. Lindquist, in Magnetism, edited by G. T. Rado and H. Shul, Vol. IIA, page 357 (Academic Press, New York, 1965).

88. e.g., R. M. Bozorth, Ferromagnetism (D. Van Nostrand Co., New York, 1964).

89. G. J. Perlow, Phys. Rev. 172, 319 (1968).

90. N. Heinman, L. Pfeiffer, and J. C. W. Ker, Phys. Rev. 184, 281 (1969).

91. S. L. Ruby and D. I. Bolef, Phys. Rev. Letters 5, 5 (1960).

ACKNOWLEDGMENTS

The author would like first and foremost to express his gratitude to the many members of the Lawrence Berkeley Laboratory staff whose help in every detail was inmeasurable.

I would like next to thank Dr. Eckart Matthias, who introduced me to experimental physics and the tantalum case, and Professor David A. Shirley for his interest and support throughout my years with the Laboratory.

It is a pleasure to acknowledge the help and friendship of Dr. Günter Kaindl, who acquainted me with the finer aspects of Mössbauer spectroscopy and provided an example to follow in his many laboratory and scientific skills.

During the years, I also had the pleasure to accomodate the help and advice of the many guests to Professor Shirley's group. In particular, I would like to mention Drs. Helmut Gabriel, Cristian Sauer, Heinz Haas, H. Eberhart Mahnke, and Herbert Rinneberg.

My fellow graduate students, past and present, deserve special gratitude for their help and encouragement against many odds and trying times, and above all for their friendship. I would especially like to mention John A. Barclay, Stephen S. Rosenblum, Arthur J. Soinski, Raymond Dod, William D. Brewer, Fredrick Bacon, Thomas A. Koster, Donald W. Davis, Roger A. Pollak, and Richard W. Streater, with whom I also spent time discussing many topics.

Great appreciation for their constant and immediate help in matters of chemistry, safety, and technology, are extended to Mrs. Winifred Heppler, Mrs. G. R. Bolz, and Mr. Dimitri "Ed" Voronin, respectively, who truly are the "wunder" people of the group.

Many of my friends outside the laboratory, have also offered me encouragement and relief. In particular, I would like to thank my friends with whom I spent many-a-day hiking and ski-touring in the mighty Sierras. Of special mention are also my dear friends Susan Benson and Susan Jamart.

Finally, I would like to thank my parents, Kurt and Regina R. Salomon, and my sister, Jill Salomon, for their confidence in me, and their encouragement and support throughout my educational career.

The financial support of the United States Atomic Energy Commission is gratefully acknowledged.

LEGAL NOTICE

This report was prepared as an account of work sponsored by the United States Government. Neither the United States nor the United States Atomic Energy Commission, nor any of their employees, nor any of their contractors, subcontractors, or their employees, makes any warranty, express or implied, or assumes any legal liability or responsibility for the accuracy, completeness or usefulness of any information, apparatus, product or process disclosed, or represents that its use would not infringe privately owned rights.

TECHNICAL INFORMATION DIVISION
LAWRENCE BERKELEY LABORATORY
UNIVERSITY OF CALIFORNIA
BERKELEY, CALIFORNIA 94720